THESIS FOR THE DEGREE OF LICENTIATE OF ENGINEERING

Nanobubbles in water - how to identify them and why they are stable

FREDRIK EKLUND

Department of Physics

CHALMERS UNIVERSITY OF TECHNOLOGY

Gothenburg, Sweden 2019

Nanobubbles in water - how to identify them and why they are stable

FREDRIK EKLUND

Department of Physics
Chalmers University of Technology
SE-412 96 Gothenburg
Sweden
Telephone + 46 (0)31-772 1000

Cover:
The authors rendition of laser holography and light scattering.
The green laser beam is being scattered by a bubble.
The red laser beam speeds up when passing through an air bubble, whereas the speed of light is lower in water.
The resulting phase shift can be detected by digital holography.
Based on a bubble image from Vectorstock, NZ.

Chalmers Digitaltryck
Gothenburg, Sweden 2019

Nanobubbles in water - how to identify them and why they are stable

Fredrik Eklund
Department of Physics
Chalmers University of Technology
SE-412 96 Gothenburg
Sweden

Abstract

Gas bubbles smaller than 1 micrometer in water, commonly referred to as nanobubbles, is a growing field of research and innovation. Applications range from medical imaging and drug delivery to mining industry and environmental remediation. There are many possibilities but important questions remain – how is it possible for small gas bubbles to be stable against dissolution and how can they be detected and differentiated from solid particles and oil droplets ?

In this work we demonstrate that several common nanobubble generation methods can generate contamination particles which can be mistaken for bubbles and that with sufficient cleanliness, neither particles, droplets or bubbles are generated. Theories on nanobubble stability that does not include impurities can thus be dismissed. (Paper 1). Lipid stabilization and the dynamic equilibrium model based on hydrophobic dirt particles appear to be the only valid models for nanobubble stability at present.

We furthermore demonstrate Holographic Nanoparticle Tracking Analysis (H-NTA) as a powerful new method to detect and differentiate between nanobubbles and nanoparticles in the same solution (Paper 2). As H-NTA determines the refractive index of tracked objects, bubbles will differ very significantly from solid particles or oil droplets. The refractive index of a bubble also indicates the amount of adsorbed material as well as possible clustering of multiple bubbles. The method also powerfully enables detection of different particle populations close in size and refractive index in a dispersion. The size range is 0.3-0.4 μm to 1.5 μm.

List of publications

Paper I. Stable air nanobubbles in water - the importance of organic contaminants

Fredrik Eklund, Jan Swenson

Langmuir 2018, 34, 11003-11009

Paper II. Size and refractive index determination of nanoparticles and nanobubbles by Holographic Nanoparticle Tracking Analysis

Daniel Midtvedt, Fredrik Eklund, Erik Olsén, Benjamin Midtvedt, Jan Swenson, Fredrik Höök

In manuscript.

Contributions

Paper I.

I suggested and performed all experimental work and was the main author of the manuscript.

Paper II.

I suggested and prepared the samples and performed the reported measurements. I also contributed to developing the method, primarily as a user and addressing some practical hardware issues. I wrote a substantial part of the manuscript, in particular the bubble related sections. Shared first-authorship.

Table of contents

1 Introduction

Micro- and nanobubbles in water is a rapidly increasing research topic. The interest is fuelled mostly by the many existing and potential technical and medical applications and there is plenty of industrial innovation activity in this field. Microbubbles (fine bubbles) are used since many years as contrast agent in medical ultrasound imaging[1] and are now being explored also as a drug delivery vehicle. Industrially, microbubbles are used in water purification[2] and for separation processes in the mining industry[3]. In recent years, a large number of small innovation companies have developed different ways to generate smaller bubbles (ultrafine or nanobubbles) and explored new areas of use. Nanobubble technology has been applied in cleaning[4], fish farms and agriculture[5], environmental remediation[6], disinfection[7] and more. The possibilities seem endless and the future bright. However, the understanding of the properties of nanobubbles remains limited and in some cases there is even reason to doubt scientific reports as well as commercial claims.

Besides artificially generated bubbles, small gas bubbles do already exist in water naturally. These bubbles affect common phenomena such as cavitation and boiling. The existence of small gas bubbles in water has been known for a long time, in older literature these are referred to as “cavitation nuclei”. Water without any such “nuclei” behave considerably different from normal water in that formation of larger, macroscopic bubbles is considerably more difficult when gaseous “nuclei” are not present. Therefore, nuclei-free water can be heated to considerably higher temperatures than 100°C before bursting into a boil.

Another role which bubbles play in nature is in the gas exchange between the atmosphere and the ocean. Bubbles, small and large, have a large impact on the dissolution of atmospheric gases, including CO_2 in sea water and need therefore to be taken into account in research on climate and ocean acidification[8]. Recently, nanobubbles were suggested to be of vital importance in the life of trees[9]. The theory is that air released by the extreme subpressures in tree sap forms nanobubbles rather than macroscopic bubbles which would block the flow. As bubbles are present everywhere, they may play many more

roles in nature which we are presently not aware of. Understanding nature thus provides a second motivation for the study of very small bubbles.

Whereas many technical designs for "bubble generators" have been developed, there is still a fundamental lack of knowledge about the bubbles themselves and what factors are necessary for their stability. Theoretically, a very small air bubble in water should dissolve almost instantly, but something often stabilizes them for hours and days. This thesis is partially a search for this "something".

Furthermore, the study of bubbles smaller than 1 μm faces some difficulties due to that detection and measurement of these bubbles is not entirely straightforward. Several commonly used methods for detection of solid particles and droplets in liquids cannot differentiate between particles, bubbles and droplets. Many methods have been suggested to differentiate between bubbles and particles, some of these have been explored in this work.

2 Historical and technical background

2.0 Overview

With improved light scattering instruments, many researchers discovered unexpected submicron particles in various aqueous solutions during the late 90s and early 2000s[10-13]. Such particles were sometimes interpreted as "solute clusters", loose aggregates of dissolved substances. Sometimes they were interpreted as "nanobubbles" of air. These interpretations were probably not always correct in either case. At the same time, Atomic Force Microscopy (AFM) became better and more affordable and scientists discovered submicron particles on hydrophobic surfaces in water, which were also interpreted as bubbles of air[14, 15]. Free floating "bulk nanobubbles" and interfacial- or surface nanobubbles initially progressed as two rather separate research areas. Surface nanobubbles initially received much more attention as they were easy to generate repeatably and to study with AFM, and probably also since the existence of bulk nanobubbles was more questioned. As early papers on "nanobubbles" rarely reference older literature on "cavitation nuclei", there seem to have been a common unawareness of it.

The new discovery of nanobubbles fuelled plenty of innovation activity both inside and outside academia. Soon several nanobubble generators were available on the market and new applications were explored by enthusiastic entrepreneurs. Much of this innovation activity took and takes place in Japan, where the Fine Bubble Industry Association (FBIA) was formed in 2012 and as of today has 61 corporate members[16]. FBIA has initiated a comprehensive standardization work in the International Standardization Organization (ISO). One of the results from the work within ISO Technical committee 281 is a recommendation that the term "nanobubble" for bubbles smaller than 1 micron be replaced with "ultrafine bubble" as the term "nano" is generally recommended to be used for objects smaller than 100nm. For bubbles in the range 1 to 100 micron, the term "fine bubble" is recommended. In scientific literature the terms nanobubble and microbubble are however still very common, and therefore used in this thesis. The term micro-nanobubbles is also used, meaning a mixture of micro- and nanobubbles which is often the output of commercial bubble generators.

2.1 Cavitation and boiling

Although it may seem like nanobubbles were discovered in the 1990ies, there have been strong indications of their existence much earlier. Cavitation is a phenomena where locally low pressure in water causes a vapor cavity to appear, expand and collapse. Cavitation can occur around propellers or in pumps and cause erosion of metallic materials when the bubble collapse takes place at the surface. Cavitation on ship propellers was discovered in the late 1800s, although the problem had been noticed in rotating machinery much earlier[17]. It was later found that cavitation in very pure water requires orders of magnitude greater subpressures to occur, compared to "normal" water[18, 19]. It can also be shown theoretically that the tensile strength of pure water is considerably higher than what is observed in "normal" water. (By normal water is here meant for example tap water or any fresh water that has not been highly purified). Apparently, there is some kind of "cavitation nuclei" in normal water that facilitates cavitation. Fox and Herzfield speculated already in 1954 that microscopic air bubbles stabilised by an organic skin may act as a cavitation nuclei[20]. Many experiments have shown that nuclei are often spherical and in the range of a few microns to a few hundred microns[17], but without determining their exact nature. However, some claim that nuclei are

primarily submicron[21]. More recently, it has been experimentally shown that particles with interfacial nanobubbles on the surface can act as cavitation nuclei[22, 23]. Thus, it is still not entirely obvious whether bubbles on particles or free bubbles are the most important cavitation nuclei. It is however quite obvious that cavitation nuclei carry gas cavities. Pressurization and degassing has been showed to remove cavitation nuclei[18, 24, 25].

Early work with water tunnels (the equivalent of wind tunnels) found that cavitation nuclei rapidly accumulated due to cavitation and were recirculated to the tunnel entrance. A solution was found where a long return pipe at elevated pressure forced most of the "nuclei" to dissolve. Secondly, a deaerator reduced the air saturation to 20-50% in the water[26].

Already in the 1960ies several researchers showed that the presence of a small concentration of organic substances in water influenced the cavitation threshold[27]. Thus, there were early indications that bubbles are indeed stabilised by surfactants and act as cavitation nuclei.

An early interesting finding was that cosmic radiation appears to generate stable cavitation nuclei. It had already been shown that a superheated liquid was sensitive to cosmic radiation and neutron sources[28]. Superheated ether was shown to burst into boiling faster in presence of a neutron source, and boiling was also shown to be triggered by cosmic radiation. This effect was soon put into use in "bubble chambers" for detection of high energy particles which generate a trace of macroscopic bubbles along their trajectory in liquified gas. Later, water was shown to be more resistant to sonically induced cavitation when shielded against neutron radiation[29], something which has been confirmed by several authors[30, 31] and shown in other liquids[30, 32]. The cavitation nuclei generated by neutron radiation appeared to have a half-time of about 70 minutes[29]. Interestingly enough, neutron radiation has also been shown to affect the bubble-mediated long range hydrophobic attraction[33] (see also chapter 3.6). The main mechanism is believed to be that neutrons collide with oxygen nuclei, which in their turn release energy locally as they slow down, causing local heating. In addition, neutrons themselves generate gamma- and alfa radiation along their path which both generate local heating and dissociation of water molecules (radiolysis) into hydrogen and oxygen.

Like cavitation, boiling is also affected by the presence of microscopic bubbles which are needed as nuclei for macroscopic bubble formation. It was shown already more than 200 years ago that degassed water could be superheated considerably above 100°C before boiling, and the search for the "true" boiling point of water became a popular research subject at the time[34]. Boiling temperatures as high as 200°C have been reported[19]. Superheating is fairly easy to achieve with pure water and a microwave oven, and numerous accidents have been reported due to this phenomenon.

2.2 Decompression sickness

A phenomenon similar to cavitation is decompression sickness, also known as divers' disease. It is a medical condition which can affect divers and is due to formation of gas bubbles in the body when traveling from a high pressure to a lower pressure environment. Bubbles can form at different places in the body and many different symptoms can therefore arise. Most common is joint pain, which is not unexpected since the joints are known to contain gas bubbles and thus possible cavitation nuclei. In the most serious cases, bubbles are formed in the spinal cord and in the blood stream, leading to paralysis or death.

The supersaturation attainable in human blood is far too low for spontaneous bubble nucleation to occur. Pre-existing nuclei must be present[35]. Pressure treatment can destroy nuclei, which was proven in vivo on shrimp as well as rats. Exposure to high pressures before a decompression greatly reduced the number of bubbles formed and the incidence of decompression sickness. Bubble formation is believed not to take place in the cells or in the blood, but rather in places where gas is already regularly observed and where symptoms of decompression sickness are most common, namely the joints, including the spine[35]. Further evidence of this is that bubbles seem to be generated more when a suffering animal or person is moving. Arielli[36] did however observe bubble nucleation at the surface of blood vessels in water upon decompression and concluded that nucleation takes place from nuclei on hydrophobic surfaces.

Guidelines and tables for divers to avoid decompression sickness are based on empirical experience and animal testing. In later studies, bubble formation in Agarose gels was used as a model system, providing some interesting

insights[25, 37-39]. Just like in cavitation in water, bubble formation was found to depend on the presence of small gaseous nuclei. By filtering the distilled water used to prepare the gels through filters of different pore sizes, it could be concluded that cavitation nuclei had a size from 1 μm down to less than 0.2 μm[21]. The number density appeared to increase with decreasing radius.

2.3 Contrast agents

Due to the ability of bubbles to resonate with high frequency sound, they absorb and scatter ultrasound very strongly. In the late 1960s, researchers working with ultrasound imaging noticed a strong contrast enhancement when certain solutions where injected into the blood stream. It was soon found that this was due to formation of microbubbles[40, 41]. The first commercial product appeared on the market in 1990 and was soon followed by several others[42]. Early products were based on generation of air bubbles and had a very short half-life. Eventually air was replaced by fluorinated gases with very low water solubility. As these gases diffuse into the water much more slowly due to their limited solubility, this improved the half-life considerably. Other improvements for enhanced stability were the introduction of bubble shells of lipids, proteins and polymers. Microbubble contrast agents typically have a size distribution of 1-7 μm. In more recent research, microfluidic techniques have been explored for production of microbubbles as well as nanobubbles. One advantage of using smaller nanobubbles is that they can penetrate into tissue that microbubbles can not[43-45]. There is also great interest in the use of bubbles as a combined contrast agent and drug delivery vehicle[45, 46].

2.4 Other Technical applications

Froth flotation is a very important process in the mining industry[3]. The process separates hydrophobic particles from hydrophilic particles based on the fact that hydrophobic particles adsorb on air bubbles which rise to the surface and create a froth. The process requires the material to be separated to be ground to a particle size of 0.1mm or less. Mined material (ore) is typically a mixture of different minerals and flotation is a powerful method to separate them. When the desired mineral is not naturally hydrophobic, chemicals are added which selectively adsorb to the mineral of interest and render it hydrophobic. In recent years, the use of nanobubbles in addition to regular larger bubbles

has been explored[47-51]. The results indicate that enhanced flotation efficiency is possible. The mechanism is suggested to be that the nanobubbles adsorb to and coat the surface of hydrophobic particles, which enhances their adsorption to larger bubbles.

Dissolved Air Flotation (DAF) is a different flotation technique which is commonly used for purification for drinking water and waste water[2, 52]. DAF is used to remove all solids from water whereas froth flotation is normally used to separate different types of solids from each other. Whereas in froth flotation air is diffused directly into water, generating comparably large bubbles (>1mm), air is in DAF dissolved in water under pressure and bubbles of smaller size (<0.2 mm) are generated by depressurization and cavitation.

Adsorption of nanobubbles to hydrophobic particles can also be utilized in cleaning applications[4]. Adsorbed bubbles are in this case believed to keep dirt particles dispersed in solution, in a similar way as surfactants work. Commercial applications exist, but cleaning with micro- and nanobubbles is a technology still in its infancy.

Micro- and nanobubbles have successfully been used in agriculture, fish farming[5] and in environmental remediation of soil and bottom sediments[6]. In these applications, bubbles of pure oxygen are often used in addition to air bubbles, and the positive effects are probably to a large extent an effect of increased oxygen concentration in the water. It appears that micro- and nanobubbles due to their small size and long life have the ability to penetrate deep into bottom sediments and deliver oxygen, achieving results that conventional aeration techniques do not.

In addition to increased oxygen concentration, elevated concentrations of Reactive Oxygen Species (ROS) have also been detected in "nanobubble water"[7, 53]. ROS is most probably generated due to cavitation during the bubble production[54]. A collapsing cavitation bubble generates extreme pressures and temperatures which can enhance many chemical reactions, for example the production of ROS. The term ROS includes among others hydrogen peroxide, hydroxide radicals ($OH\cdot$) and superoxide radicals ($O2\cdot^-$). Through their oxidizing action these substances are harmful to living organisms and can therefore work as disinfectants. However, at very low concentrations ROS

actually stimulate cell growth and division and can therefore be beneficial[55]. Beneficial effects of nanobubbles in agriculture and aquaculture can thus be both due to increased oxygen levels and the generation of ROS. The ROS can stimulate growth of fish or plants at low concentrations as well as function as disinfectants at higher concentrations. At even higher concentrations ROS can also be harmful to plants and animals, and harmful effects of nanobubble water have indeed been reported in some cases[7].

3 Theoretical background of nanobubbles

3.1 Diffusion and bubble stability

In a frequently quoted paper from 1950, Epstein and Plesset[56] calculated the expected life time of small air bubbles in water with the help of diffusion theory. The two driving forces for diffusion to or from a bubble are the saturation of gas in the water and the Laplace pressure. Laplace pressure is the pressure difference between the inside and outside of a gas bubble due to the surface curvature and the surface tension. The surface tension acts to pull the surface together, to decrease it. This generates a force acting in parallel with the surface. When the surface is curved around an air bubble this will generate a net force acting towards the bubble. The internal pressure of the bubble generates an opposing force, balancing the force from the surface tension and the external pressure. The internal pressure of a bubble is thus the Laplace pressure plus the external pressure. The formula for the Laplace pressure of a spherical bubble is: $\Delta P = \gamma * 2/R$, where R=Radius, γ=surface tension.

If an air –water interface is clean and does not have any surfactants adsorbed, the surface tension is very high (72 N/cm). If there is no surface tension at the air-water interface, a bubble will shrink when the water is undersaturated with air and grow if it is oversaturated. However, a small air bubble with a high surface tension will have a very high Laplace pressure which will force air to diffuse from the bubble into the water even at moderate oversaturation, as can be seen in fig 1. For a clean air bubble with 1μm diameter, the Laplace pressure will be high enough (2.9 bar) to drive dissolution at up to more than 150% saturation. Saturations up to about 150% are commonly occurring in natural waters or tap water[57].

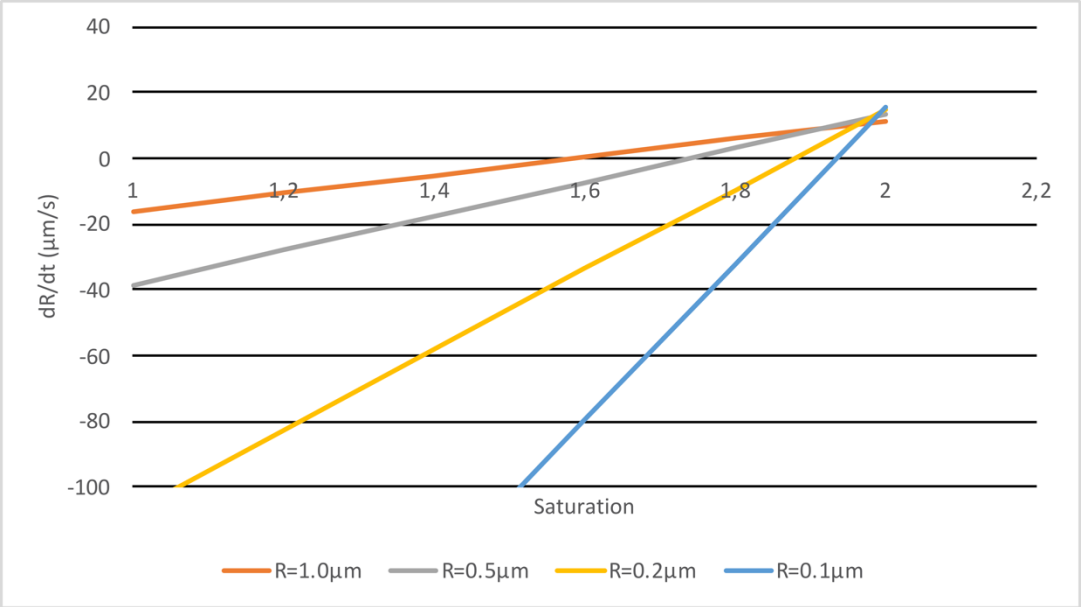

Fig 1. Rate of change in radius (R) due to diffusion for a clean air bubble in water, with a surface tension of 72N/cm and at 293K. Calculated from eq (15) in ([58]). A negative value means a shrinking bubble, a positive value means a growing bubble.

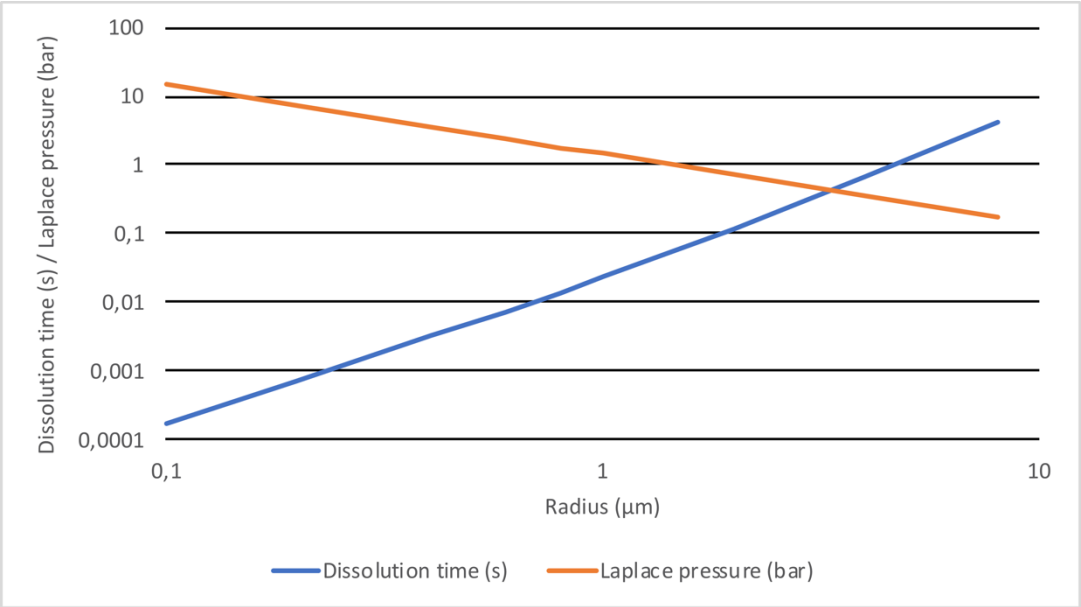

Fig 2. Blue line: Time for complete dissolution of an air bubble in water with 100% air saturation, a surface tension of 72N/cm and at 293K. Calculated from eq (17) in ([58]). Orange line: Laplace pressure under the same conditions. Both axes are logarithmic.

Epstein-Plesset made several simplifications in their analysis, and more detailed models have later been developed by others but their predictions have been experimentally confirmed with rather high accuracy (+-8% for dissolution times)[58]. Epstein-Plesset assumed the bubble to be stationary, i.e. that there is no effect from movement through the liquid. They also neglected any convection resulting from the movement of the interface due to the shrinking of the bubble. They furthermore assumed that the bubble is alone in a large volume, no other bubbles in the vicinity prevents diffusion. And importantly, air was assumed to diffuse freely across a clean air-water interface, with no diffusion barrier at the interface. This last assumption was never clearly stated by Epstein-Plesset, it was just taken for granted. However, this may not always be the case, and this may be of importance for the stability of small bubbles.

3.2 Adsorbed surfactants and bubble stability

As was mentioned in chapter 2.1, surfactant stabilized bubbles – functioning as cavitation nuclei – were proposed by Fox and Herzfeld in 1954. They suggested that the main stabilizing effect of adsorbed surfactants would be to slow down diffusion of gas, whereas the decrease in surface tension and thus Laplace pressure would be very moderate.

Later, Yount[38, 59] suggested a model for stable micro- and nanobubbles with a surfactant layer of variable permeability. In this model, the skin of adsorbed surfactants would normally be permeable to gas diffusion, but at rapid compression the skin would become almost impermeable. Furthermore, this model suggests that the surface tension is close to zero due to the very dense packing of surfactant molecules that can be achieved on a curved surface. Yount's experiments did indicate that invisible cavitation nuclei stabilized after a rapid increase of the external pressure, but the evidence is indirect as the nuclei themselves were not detected, only the resulting macroscopic bubbles after decompression. In support of these claims, others have shown that a rapid compression of a monolayer of lung surfactant would stabilize it considerably[60].

Borden and Longo examined the permeability of a surfactant layer on a bubble attached to a microscope slide and found an increased resistance to diffusion

with the number of carbon atoms in the surfactant tail in the range from C18 to C24[61]. But with less than 18 carbons in the tail, the diffusion resistance was constant and independent of chain length. Duncan and Needham, while confirming the Epstein-Plesset model, also examined the diffusion barrier claims. They concluded that the C18 surfactant they used, DSPC, created no diffusion barrier for gas to diffuse out of the bubble. They also re-examined Borden's results and concluded that there is no diffusion barrier effect at all below C18, only at longer chain lengths. Since natural surfactants found in water to a very large extent has tail lengths of 18 carbons or less[62], it seems likely that the diffusion barrier effect would not be important for natural surfactant stabilized nanobubbles. For artificial bubbles, the effect could however be utilized and it has been shown that fatty acids with long chain lengths increased the life length of artificial contrast agent microbubbles[63]. For bubbles stabilized by random "impurity" surfactants, surface tension depression leading to a very low Laplace pressure is likely the main stabilization mechanism. This means that such bubbles can only be expected to be stable in gas oversaturated solutions.

Surfactants are often studied in Langmuir troughs, where the surfactant form a monolayer on a plane water surface. The monolayer is gradually compressed by a movable barrier and the pressure required for compression is measured. A poorly water-soluble surfactant will stay at the surface until the monolayer mechanically collapses. The surface tension can be determined by subtracting the measured surface pressure from the surface tension of the air/water interface without surfactant. This means that an interface with a low surface tension has a high surface pressure, and vice versa.

The surface tension measured on a plane water surface will not reach close to zero for a single-tail surfactant as they generally have a "conical" geometry, i.e. the headgroup occupies more space than the hydrocarbon tail. But on a curved surface, such as a bubble or an emulsion droplet, conical surfactants can pack more densely and reach a considerably lower surface tension. Double-tail surfactants, such as phospholipids which constitute a large part of cell membranes and which are used to stabilize contrast agent microbubbles, can however pack very densely on a plane interface and in some cases reach zero surface tension under compression in a Langmuir trough. Not only can

zero surface tension be reached, but even negative surface tension has been suggested for an air bubble under high external pressure[64, 65].

A surfactant monolayer can exist in different 2-dimensional phases, just like 3-dimensional materials can exist in different phases (gas, liquid, solid). When a monolayer of surfactant is compressed in a Langmuir trough, it will transition from one phase to another and this can often be seen as a stepwise jump in surface tension/surface pressure. For historical reasons the phases of a monolayer are usually denoted gas, liquid-expanded, liquid-condensed and solid. Other nomenclatures have also been used. Kaganer and coworkers suggested that the term liquid-condensed be abandoned[66] and only the term condensed should be used for liquid-condensed and solid-condensed. Instead the two condensed phases could be designated tilted-condensed and untilted-condensed, which would more accurately reflect their nature. In the condensed states the surfactant tails are aligned and organized, whereas in the liquid-expanded state they are more disordered.

The condensed states require that the interface is supersaturated with surfactant molecules[67]. Several phases may coexist in a monolayer, condensed "islands" which float in a "sea" of the liquid-expanded phase may form and gradually expand upon compression until the whole layer is condensed. To reach the lowest possible surface tension, the surfactant layer has to be in a condensed state. Surfactant stabilized microbubbles have been observed to shrink in size by a factor of 2.5 before stabilizing. This factor corresponds to what is expected from a transition from expanded to condensed state[68].

Furthermore, Yount[37] (1984) imaged bubbles in a gel with Scanning Electron Microscopy (SEM). After staining the samples with Osmium Tetroxide, which will provide contrast to organic materials, he saw a cloud of organic materials around the bubbles and concluded that a reservoir of surfactants is present and is necessary for stability.

Surfactant stabilization is well known in the field of artificial microbubbles used as contrast agents. There are also more and more papers published on artificial nanobubble contrast agents produced with similar methods and compositions. Micro/nanobubbles stabilized by unknown impurities in tap-, fresh- or sea water are still more of a mystery. Naturally occurring surfactants,

such as fatty acids, are to a greater extent single tailed and will therefore behave differently than the double-tailed phospholipids generally used in artificial contrast agents. Bubbles large enough (>0.5 μm) to be imaged by optical microscopy seems to have a smooth surface and only occasionally an attached particle[37, 69], which would speak for surfactant stabilization and against the dynamic equilibrium model (chapter 3.3). But this is only what is seen optically. Something that also speaks for surfactant stabilization is the extensive experience and research on oil-in-water (o/w) and water –in-oil (w/o) emulsions, where droplets down to considerably less than 100nm can be generated and be stable for long periods of time. In these cases, very low surface tensions can be achieved on small droplets, using single-tail surfactants. For bubbles, diffusion of its contents into the bulk water is a greater problem than for oil droplets, but in the case of oversaturated water the similarities with o/w emulsion droplets should be very significant.

3.3 Dynamic equilibrium model for bulk nanobubbles

Recently, a dynamic equilibrium model was suggested[70], wherein adsorbed hydrophobic substances are proposed to stabilize bulk nanobubbles. A similar model had previously been suggested for surface nanobubbles (see 3.5). In the present model, the adsorbed substances are completely hydrophobic, without any hydrophilic surfaces. Since gas is attracted to hydrophobic surfaces, it was suggested that a steady inflow of gas is generated at the edges of the hydrophobic material which is balanced by the diffusional outflow of gas from the non-covered parts of the bubble surface. An important feature of this model is that it predicts that bubbles can be stable not only in oversaturated, but also in slightly undersaturated water (80% saturated). The surface coverage needs to be only 50% for stable nanobubbles and much less ($3x10^{-4}$) for bubbles of 2μm radius. The authors claim the model is valid for rigid material as well as flexible material such as oil. Experimental support for this model is provided by a recent paper[71] where nanobubbles were generated in water with added hydrocarbons or fatty acids. The nanobubble samples were imaged by Transmission Electron Microscopy (TEM) in liquid state in a narrow channel, images show droplets of oil on the surface of apparent air bubbles. It has also been shown that bulk nanobubbles can indeed be generated and survive in mildly gas undersaturated water[72].

3.4 Other theories on bulk nanobubble stability

It has been claimed that inorganic ions alone can stabilize nanobubbles, even at concentrations as low as 10^{-6}M [73]. The idea is that selectively adsorbed anions create a coulombic repulsion, which counteracts the pressure from the surface tension. This idea has been questioned based on; 1) The charges when compressed should diffuse in to the liquid rather than stay at the surface and generate a pressure along the interface[74], 2) The pressure from the ions has been calculated to be negligible compared to the other forces at work[54]. Other authors have also claimed that addition of salt helps stabilizing nanobubbles[75] and based on this, it has become popular among researchers to add NaCl to water when performing nanobubble experiments. One possible explanation why inorganic salts may benefit nanobubble stability is that salts will decrease the solubility of surfactants, the so-called salting-out effect. As mentioned above, bubbles are likely stabilized by poorly soluble surfactants, and salt may push slightly soluble surfactants to become insoluble. Salt may also affect the repulsion between bubbles and thus the probability of coalescence. Higher salt concentrations will however shield surface charges and decrease the zeta-potential, which will increase coalescence. This has indeed been found experimentally[75, 76] for bubbles.

Based on ATR-IR measurements[77] and Raman measurements[78] on nanobubbles in distilled or deionised water, it has also been suggested that a specific water structure at the air-water interface prevents gas diffusion.

3.5 Additional factors for bulk nanobubble stability

Once the bubble is stable against diffusion, other factors become important for bubble stability. Buoyancy is one such factor, a clean bubble will acquire buoyance already at a size below 1 μm and slowly rise to the surface. This means that a bubble needs to be sufficiently small to be stable. The critical size can be larger if there is heavy material adsorbed to the bubble.

Another important factor is, as mentioned above, surface charge or zeta potential. A high zeta potential can prevent coalescence of bubbles and is thus a potentially important factor. Zeta potential is dependent on pH and salt concentration the effect of these factors has been investigated in several

nanobubble papers[75, 76, 79-81], although many of those papers failed to ascertain that the bubbles were actually bubbles.

3.6 Surface bubble stability

3.6.1 Bubbles on flat surfaces

Nanobubbles on surfaces have been experimentally and theoretically investigated in many papers. Since dissolved gas has an affinity for hydrophobic surfaces, formation of nanobubbles occurs much more readily on such surfaces, although they have been observed also on hydrophilic surfaces. Several mechanisms have been proposed and the one that appear most accepted[82, 83] stresses the importance of pinning of the contact line of the bubble. Pinning requires that the surface is not perfectly smooth. The pinning has also been shown to be destroyed by addition of surfactants. The pinning stabilization model states that the outflow of gas due to Laplace pressure is balanced by the inflow of gas due to oversaturation and that this balance is achieved at a certain contact angle. The contact angle is thus dependent on the degree of oversaturation and these low contact angles require contact line pinning, without which the contact angle would be greater. The model matches experimental findings of generally low contact angles and that irregularities on the surface are beneficial for stable bubbles to form.

The above model states that surface nanobubbles can only be stable in oversaturated water. Very recently, a modification of this theory was proposed[84], where the affinity of gas to hydrophobic surfaces was also taken into account, predicting stable surface nanobubbles to be possible also in slightly undersaturated water. This model also states that oversaturation and hydrophobicity are not simultaneously necessary, only one of these criteria is necessary for surface bubble stabilization. This model also matches experimental findings that bubbles are stable over long time in open systems and react remarkably slowly to degasification. It also matches experimental observations of bubbles on hydrophilic surfaces. Tan effectively reintroduces the dynamic equilibrium model, but combines it with the contact line pinning model. Lohse, who previously abandoned the dynamic equilibrium model, now in principle accepts Tan's combined model*.

*Statement at Nanobubble 2018 conference.

3.6.2 Bubbles on particles

Early on in cavitation research, cavitation nuclei were suggested to consist of solid particles with air pockets in cracks and crevices[18, 85]. More recent research has confirmed that particles can act as cavitation nuclei[22, 23, 86-88] and that after several cavitation events the particles ability to nucleate bubbles is exhausted, evidencing that air bubbles on the particles are the actual nuclei. Different particles have a widely varying ability to nucleate cavitation and this seems to be related to surface structure[22], size[86] and hydrophobicity[23]. A rough surface structure is more important than deep pores, which suggests that bubbles are located on the particle surface rather than in cracks and pores, and are pinning-stabilized similarly as bubbles on a flat surface. Smooth larger particles (76μm) were shown to be more nucleating than smooth small ones (3μm), also indicating surface bubbles. What also speaks against the crack/crevice model is that bubbles in cracks are very small, whereas they need to be of a minimum critical size in order to nucleate cavitation[87]. The crevice model has been confirmed by cavitation experiments with etched 50nm wide cylindrical pits on a flat hydrophobized silica surface. Cavitation could be nucleated only once per pit[89]. The experiments fitted well with the theoretically expected relation between pit size and the pressure amplitude necessary to generate cavitation. For cylindrical pits of 50-60 nm diameter, the required pressure pulse amplitude is very high, 20-30 bar. For more moderate pressure amplitudes, larger pits are required for nucleation. Thus, the crevice theory holds well for cavitation at macroscopic surfaces – where indeed cavitation is more commonly observed than in the bulk of the liquid, but not so well for colloidal particles. Water need (according to some) to be filtered at 1 μm or less to increase its resistance to cavitation and if particles are responsible, such small particles cannot have crevices of several hundred nm diameter. It is important to keep in mind that particles not only may have small bubbles on their surface, bubbles can also have small particles on their surface. Particles can act like surfactants and adsorb to the air-water surface. Particles which are partly hydrophobic, partly hydrophilic are particularly surface active. For this reason, some cavitation experiments with particles can be interpreted in different ways. But in some studies, cavitation events at a single particle have been imaged with microscopy.

3.7 Nanobubbles and the hydrophobic attraction

Attraction between hydrophobic molecules or parts of molecules is a well-known and important phenomenon, but from the early 1980s[90] and onwards there were also numerous reports of a long-range attraction between surfaces. This force seemed to have two different regimes, a longer range from 25nm to 100nm or more, and a shorter range from 10-25 nm. The research of this long-range hydrophobic attraction was actually what eventually led to the discovery of surface nanobubbles. The long-range hydrophobic force turned out to be not an actual force, but due to bridging of pre-existing nanobubbles on the hydrophobic surfaces[15, 91]. This explained why the effect was poorly reproducible. It was shown that the attraction decreased to varying degree if the water was degassed. Furthermore, studies using AFM have shown a repulsive force preceding an attractive jump. The initial repulsion was shown to be pH dependent, which indicates that it is due to electrostatic repulsion between charged bubble surfaces. The charge of a surface in water (Zeta potential) usually varies with pH, being negative at high pH, positive at low pH and zero at some point in between.

Interestingly, the long-range hydrophobic attraction has in one paper been shown to be influenced by neutron radiation[33]. This further confirms the bubble generating effect of neutron radiation, mentioned in chapter 2.1. Neutron irradiation of the solution prior to injection in the sample cell enhanced the magnitude and distance of the attractive force. This could mean that bubbles generated in the bulk of the solution by neutron irradiation adsorb to the surface and enhance the long-range hydrophobic attraction.

The shorter-range hydrophobic attraction at decay lengths of less than 25 nm is more mysterious and believed to have other causes. Degassing was shown not to affect the short-range attraction[92]. A recent review states that evidence for short-range hydrophobic attraction in the range 5 - 25nm is scarce[93]. After 30 years of research there is only two papers that show such an effect unambiguously, according to this review.

Very recent work does however provide further evidence of a hydrophobic attraction force in this range[94-97]. Ishida and coworkers showed the force to increase monotonously with increasing hydrophobicity (measured contact

angle) of the surface. They cautiously suggest that cavitation between the surfaces is responsible, thus gas would be involved also in this case. Schlesinger showed the force to be diminished by degassing and went on to provide evidence of a thin layer of adsorbed gas molecules at a hydrophobic surface.

Practically, Pashley showed[98] that oil could be stably emulsified in water without addition of any surfactant if the water was degassed very thoroughly beforehand. The degassing took place by repeatedly freezing and thawing the water under vacuum, a well-known method to reach very low concentration of dissolved air. By removing the air, the attraction between the hydrophobic oil droplets decreased since no bridging bubbles were present to help them agglomerate and coalesce. Pashley later went on to demonstrate an enhanced cleaning ability of such degassed water[99].

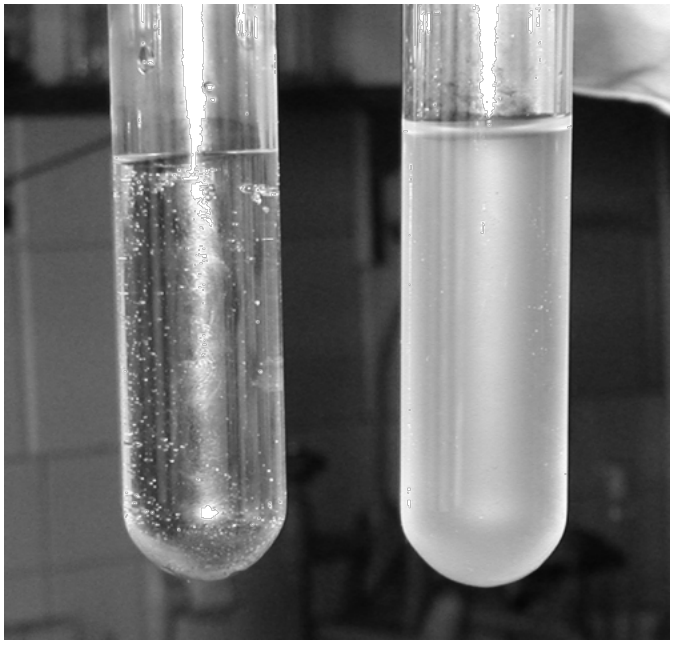

Fig 3. Photograph of gassed (left-hand side) and de-gassed (right-hand side) water shaken vigorously with oil (perfluorohexane). Reprinted with permission from R. M. Pashley, M. Rzechowicz, L. R. Pashley, M. J. Francis, De-Gassed Water Is a Better Cleaning Agent, J. Phys. Chem. B 109 (2005) 1231-1238. Copyright (2005) American Chemical Society.

3.8 Bubbles under pressure

Destruction of bubbles by pressure treatment can be used to differentiate bubbles from other light scattering particles and droplets. There are many

reports on destruction of micro- and nanobubbles by pressurization, although some of them are indirect evidence in cavitation experiments where the character of the "cavitation nuclei" is unknown. Some of these reports were mentioned in chapters 2.1 and 2.2. It is not entirely obvious how bubbles are destroyed by pressurization as several mechanisms are possible. Johnson and Cooke[69] observed bubbles in the size range 0.5-10 μm in an optical microscope. The bubbles were generated in sea water and stabilized by adsorbed impurities. Upon a pressure rise by only 0.083 bar, many, but not all, bubbles rapidly dissolved. Smaller bubbles were to a greater extent unaffected. A pressure increase by 0.14 bar removed all visible bubbles. These bubbles were apparently less resistant to pressure than in many other reports. More recently the number of nanobubbles, as measured by a particle counter, were shown to be reduced after exposure to 2.4 bar pressure[100] and as measured by NTA to be reduced after 500 bar[101]. These nanobubbles were generated in more or less pure water and any stabilizing contamination is unknown. The average size increased after pressurization and the maximum effect was achieved after 10 minutes. The number reduction and size increase appeared to be somewhat lower after 60 minutes pressurization than after 10 minutes.

Monolayers of surfactants are well known to wrinkle and fold under pressure on a flat surface in a Langmuir trough as well as on a microbubble shrinking by diffusion[61, 102]. When a microbubble after several wrinkling-induced collapses reaches a size of 1-2 μm, it appears to be considerably more resistant to further wrinkling. It seems likely that at some size a bubble will be too small to have room for any wrinkles. Thus, a large lipid-coated microbubble can be expected to undergo wrinkling induced collapse under moderate external pressure, but a smaller one will be considerably more resistant to collapse. Smaller lipid-coated bubbles will instead experience a compression of the lipid monolayer. In a recent paper[64], about 1 μm large lipid-coated C_3F_8 bubbles were measured by DLS while the pressure was increased from 1 to 5 bar. The bubbles were seen to decrease in size upon compression and increase in size again following decompression. The size increase after decompression was however only temporary, within minutes the size decreased back to similar magnitude as under compression. It appears that in this case the bubbles were destroyed during the decompression rather than during compression. It is possible that if the lipid monolayer was damaged after decompression, and the

liquid was oversaturated with gas, some of the bubbles grew and acquired buoyancy and disappeared from the solution. This can be seen as a cavitation event. The authors furthermore concluded that the surface tension became negative during compression, which made the bubbles to some extent resist compression. They estimated the surface tension to -15 mN/m, and the Laplace pressure to -0.8 bar. This means that there is a sub-pressure in the compressed bubble, which implies that when the lipid shell opens up during decompression, more gas will diffuse into the bubble.

Yount on the other hand, studying "cavitation nuclei" in the range 0.1-1.0 μm in agarose gel, considered the speed of compression important more important than the total pressure magnitude for destruction of nuclei[25]. A stepwise compression was shown to destroy fewer nuclei than a single pressure increment of the same total magnitude.

It should also be considered that an increase in pressure of several bar can take the liquid from a state of supersaturation or saturation, to a state of considerable undersaturation according to Henry's law. This can provide a considerable driving force for diffusion from the bubble and thus dissolution. A negative Laplace pressure, as reported by Alheshibri, can to some extent balance this driving force for dissolution, but not fully cancel it. If there is air/gas available on top of the liquid, it will eventually diffuse into the liquid and saturation at the elevated pressure will occur. Decompression will then yield a considerable oversaturation which can generate cavitation/macroscopic bubbles or micro/nanobubbles. Generation of macroscopic bubbles will deplete cavitation nuclei, i.e. nanobubbles, but there are also reports of generation of nanobubbles following pressurization and slow decompression[72]. Macroscopic bubble formation is encouraged by rapid decompression which is well known in the case of decompression sickness.

The issue of diffusion and oversaturation complicates matters and suggests that for destruction of nanobubbles, short pressurization times and rapid decompression is most suitable. In water which is free from stirring and convection, the rate of change of the concentration of dissolved gas is governed by diffusion, which is described by Fick's 1st and 2nd law. From Fick's second law it can be calculated that oxygen molecules will take 14 h to diffuse 1 cm in water.

3.9 Bubbles under vacuum

In addition to elevated pressure, vacuum can also be used for destruction of bubbles and thus to differentiate bubbles from other light scattering particles and droplets. Johnson and Cooke, who also observed bubbles under pressure, observed bubbles in sea water in the size range 0.5-10 μm in an optical microscope at mild subpressure[69]. The bubbles expanded under sufficient subpressure and most bubbles returned to their previous size when the pressure was returned to normal. Some did however proceed to shrink and disappear following this vacuum treatment. Overton[103] observed an increased resistance to cavitation for several different water qualities following degassing by heating under strong vacuum (2.7mbar), which was interpreted as due to destruction of gaseous cavitation nuclei. In recent years some authors have used various vacuum treatments to degas the solvent prior to bubble generation to prove the bubble nature of light scattering objects[72, 104, 105]. Others have vacuum treated probable bubbles in solutions, with varying results[106-108]. Zhou and coworkers found that microbubbles disappeared after 1h at 0.05 bar, but not nanobubbles. Addition of degassed water to a bubble solution has also been used[109] as a means of destroying bubbles by causing air undersaturation. Vacuum degassing has also been applied to surface nanobubbles[72, 110, 111]. Fang and coworkers recently generated both surface and bulk nanobubbles by applying mild vacuum (0.5 and 0.1 bar respectively) for short time. Surface nanobubbles were generated after 5 min vacuum, but disappeared again after 20 min vacuum. Bulk nanobubbles increased in number for 20 min, but disappeared after longer time under vacuum. In both cases much fewer bubbles were generated if the water had been degassed by freeze-thawing at 0.1 bar. To conclude, nano- and microbubbles can increase in size[69] or be generated by mild vacuum[72] for short time. After longer time under vacuum they will however be destroyed due to high undersaturation of gas. To destroy bubbles by causing undersaturation under vacuum, long time and either small distance for the air to diffuse from the bulk of the liquid to the surface, or stirring or convection is beneficial.

4 Experimental methods

4.1 Theoretical base of experimental methods

4.1.1 Light scattering theory

Measurement methods based on light scattering are the most commonly used for determining the size and concentration of particles, bubbles and droplets in water. Bubbles, particles and oil droplets, etc, hereinafter named "particles" for simplicity, will always scatter light. Even individual molecules scatter light, giving rise to a measurable background scattering signal from pure solvents.

How particles scatter light depends very much on their size, and different laws govern different size ranges. Very large particles behave rather similarly to any macroscopic surface. They will scatter light of different wavelengths similarly. Very small particles, with a diameter less than 1/10 of the wavelength of the incident light, exhibit Rayleigh light scattering. In this size range, the scattering intensity is the same in the forward and backward direction. The scattering intensity at 90° is half of that in the forward and backward direction.

The intensity of scattered light from a spherical particle in the Rayleigh region is given by[112]:

$$I_S = \frac{8\pi^4 n R^6}{\lambda^4 r^2} \left| \frac{m^2 - 1}{m^2 + 2} \right|^2 (1 + cos^2\theta) I_i$$

Where theta is the scattering angle, N is the refractive index of the medium, m = n1/n2 the ratio between the refractive index of the particle and the medium, R is the radius of the particle, λ is the wavelength, r is the distance from the particle to the point of observation. The equation assumes that the incident light is unpolarized.

As can be seen, the scattering intensity is strongly dependent on the particle size ($\sim R^6$). It is also strongly dependent on the wavelength ($\sim \lambda^{-4}$), a particle will scatter blue light 6 times more than red light. In an everyday context, Rayleigh scattering is very visible. The blue colour of the sky is due to blue light being scattered by air molecules in the atmosphere.

When the particle diameter is 1/10 to 1/1 of the wavelength, the particles are said to exhibit Mie scattering. Mie theory is however also used to describe scattering also for considerably larger particles, up to tens of μm in diameter. The Mie theory is essentially a solution to Maxwell's equations for scattering of a sphere. It is rather complex and custom software is used for calculations, as a single formula is not enough to describe it. In the Mie scattering range, the scattering intensity is not monotonically increasing with particle size due to resonance effects, and the size dependence and wavelength dependence is considerably weaker than in the Rayleigh region. Forward scattering is stronger than backward scattering. As the scattering intensity for small particles is higher for shorter wavelengths, green and blue lasers are most commonly used in modern light scattering measurement equipment.

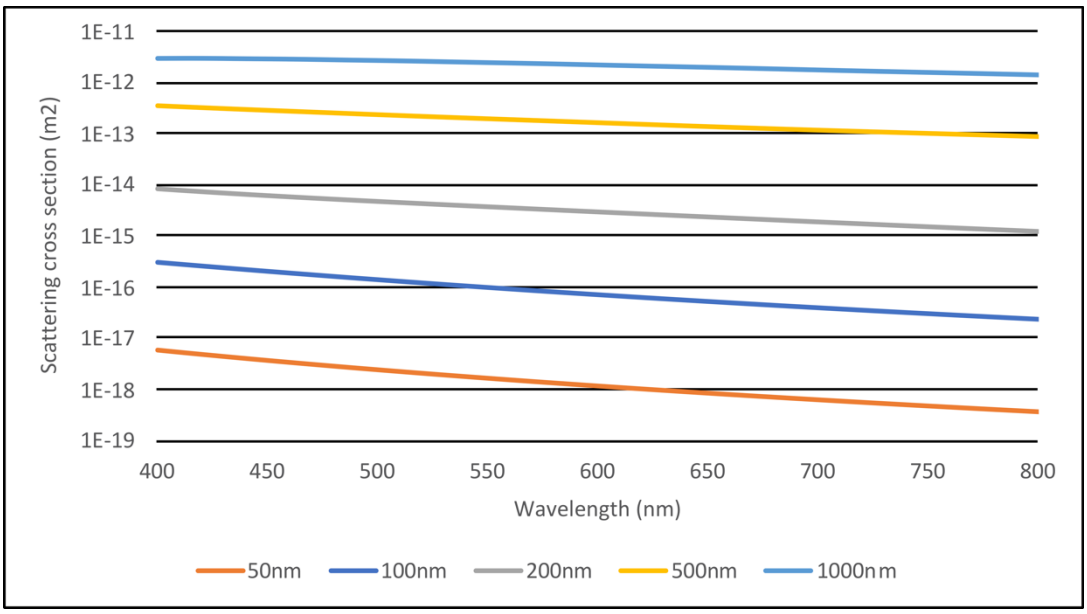

Fig 4. Calculated Scattering cross section vs wavelength for Polystyrene Latex Particles of different sizes.

Light scattering intensity is also dependent on the difference in refractive index between a particle and the surrounding medium. This is valid also if the refractive index of the particle is lower than the medium, as is the case for gas bubbles in water or other liquids. The refractive index difference for a gas bubble in water is 1.00 (air) - 1.33 (water) = -0.33. For comparison, the difference for Polystyrene latex particles is 1.59-1.33 = 0.25. A single clean air bubble can thus be expected to scatter light more strongly than a PSL particle,

which is already a comparably strong scatterer. Other commonly measured particles such as silica (1.44), biological cells, proteins and extracellular vesicles, are considerably weaker light scatterers.

4.1.2 Brownian motion

Very small particles in a liquid or in a gas will move around randomly, this movement is referred to as Brownian motion after botanist Robert Brown, who studied the phenomena extensively[113]. Albert Einstein published a landmark paper in 1905, theoretically explaining how random collisions between the particle and the molecules of the surrounding medium would occasionally be non-uniform for sufficiently small particles, causing the particle to move in random directions. The molecules in the surrounding medium will move faster with higher temperature, thus creating stronger movement. Furthermore, a smaller particle and a lower viscosity of the medium will allow faster movement. The diffusivity or diffusion coefficient of a particle is:

$$D = \frac{k_B T}{6\pi\eta R}$$

where k_B is Boltzmann's constant, T the absolute temperature, η the viscosity of the liquid and R the hydrodynamic radius of a spherical particle. This formula is referred to as the Stokes-Einstein relation. Interestingly, the diffusivity is independent of the mass of the particle. D can be seen as a measure of the positional fluctuation of the Brownian particle[113].

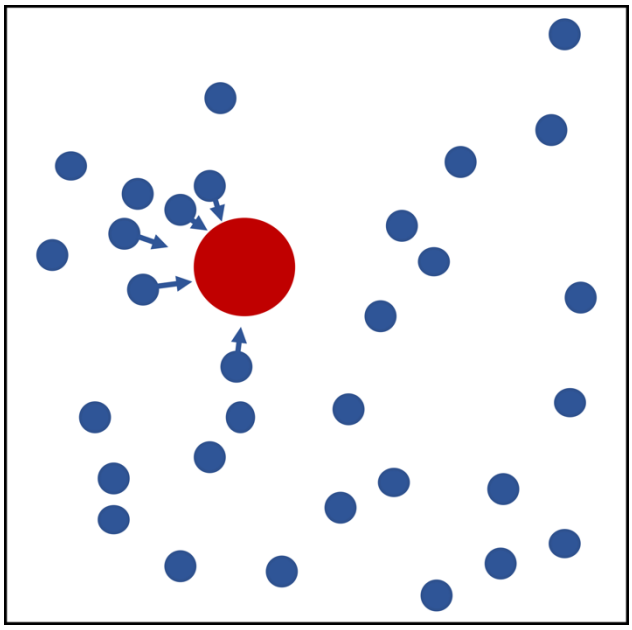

Fig 5. Conceptual image of an inhomogeneous distribution of molecules (blue dots) bouncing against a particle (red), which will cause it to move.

4.2 Dynamic light scattering (DLS)

Dynamic Light Scattering (DLS), also known as Photon Correlation Spectroscopy (PCS) is a rather mature technology. It has been used since the 70'ies and had its great commercial breakthrough in the 1990'ies. Its' progress has benefitted greatly from the rapid increase in computational capacity available. A liquid sample is illuminated by a laser and a detector is placed at a certain angle in relation to the laser beam. The detector is highly sensitive, it is essentially counting individual photons. Due to interference between light scattered by different particles, a speckle pattern will be generated in the scattered light. Due to the Brownian motion of the particles, this speckle pattern will exhibit fast fluctuations. Over a larger area these fluctuations will average out, therefore the detector measures the photon count rate or scattering intensity for a very small area[114].

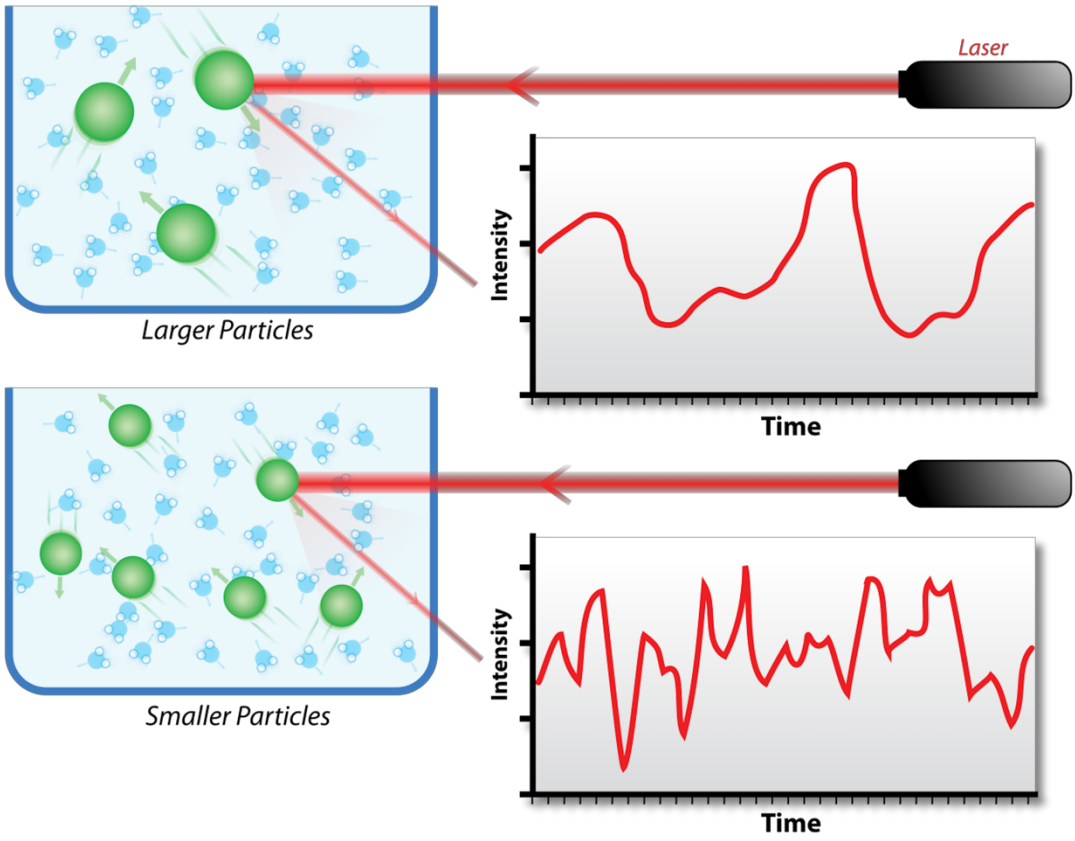

Fig 6. Fluctuations in scattering intensity from large and small particles. Image by Mike Jones, original work for Wikipedia, distributed under a CC-BY 2.0 license.

This time-varying signal can be translated into a correlation function, where the scattering intensity at an arbitrary time (t) is correlated with the scattering intensity after a time increment Δt. Thus, the correlation between the scattering intensity at time (t) and time (t+Δt) is calculated for a wide range of Δt. A plot of the normalized correlation function versus Δt will show a decay from a value close to one at small Δt, to zero at large Δt. The Δt at which the correlation function decays will be correlated to the particle size.

For a monodisperse sample of spherical particles, the correlation function will be proportional to $e^{-Dq2\Delta t}$, where q is the scattering vector and D is the diffusion coefficient of the particles. From this, D can be calculated, and with knowledge of the viscosity of the liquid and the temperature, the particle radius can be calculated from the Stokes-Einstein equation.

For a polydisperse sample, the decay will be more stretched out. There are several mathematical methods which deals with such data to interpret the correlation function into a distribution of sizes. But as DLS is a statistical method based on the mixed scattering signal from a large number of particles simultaneously, it has limited ability to determine in detail a distribution of different particle sizes. As a rule of thumb, DLS cannot distinguish a mixture of two different size populations where the size of the larger particles is less than three times the size of the smaller particles. Thus, a mixture of monodisperse 50nm and 100nm particles will look like one single population with sizes in the entire range, and an average particle size somewhere in between 50 and 100nm.

Small particles in the Rayleigh scattering region will scatter with equal intensity in the forward and backward direction, whereas with increasing size the forward scatter will be relatively stronger than the backscatter. This can be utilised by selecting a scattering angle where the particles of interest give the best signal. For small particles, interference from larger particles can be avoided by measuring at high scattering angles. For large particles a stronger signal, if desirable, can be achieved at low scattering angles.

DLS can be used over a large size interval, from molecules of single nm size to several μm. The concentration range is strongly dependent on the particle size. The upper concentration limit is limited by the sensitivity of the detectors which can be destroyed by strong light scattering, as well as by multiple scattering which can seriously skew the results. Multiple scattering is when scattered light by one particle is scattered a second time by a second particle.

4.2.2 DLS instrument - ALV-CGS-8F

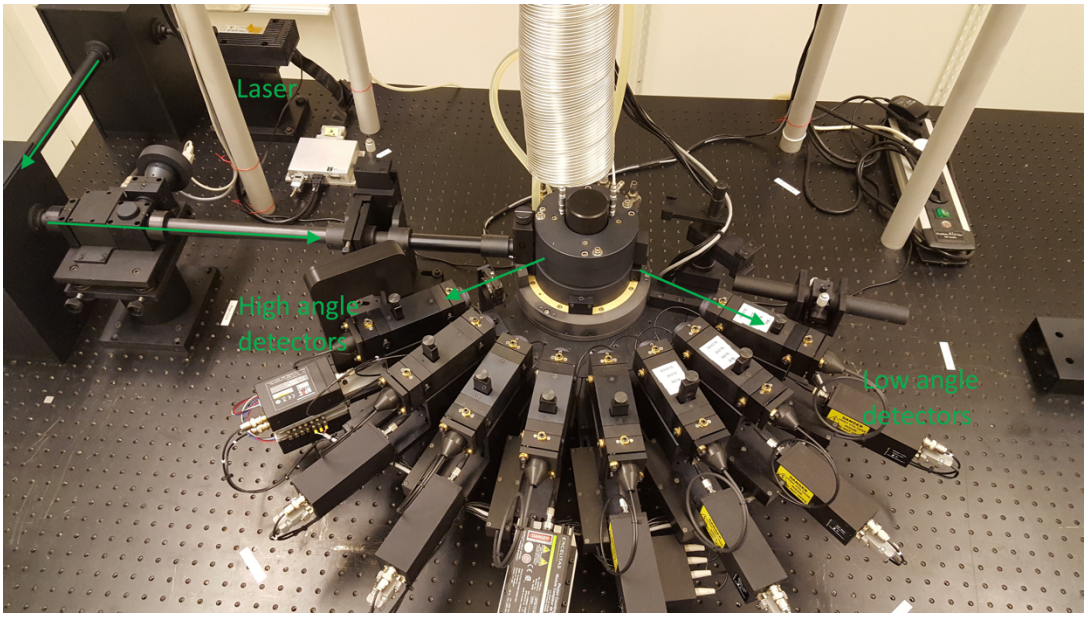

Fig 7. ALV-5000

The customized ALV-5000 is a research-type instrument with 8 detectors. The light generated by the laser (Oxxius 532S-50-COL-OE, 532 nm, 50 mW output power), passes two mirrors, followed by an automatic attenuator which can adjust the power of the beam that reaches the sample. This feature is to protect the detectors from too intense light which can destroy them. The laser beam then impinges on a cylindrical 8mm cuvette containing the liquid sample. The cuvette is placed in a cylindrical glass container filled with toluene. Toluene has a similar refractive index as the glass, which limits spurious scattering from the wall of the cuvette. This feature is primarily important for static light scattering, where the angle dependence of the scattered light is analyzed, whereas for DLS it is of less importance. The side of the vat is visible from the detector side. The detectors are mounted 17° apart and the entire set of detectors can be moved to cover a wide range of scattering angles. The detectors are PM-tubes from Perkin-Elmer (MP963). The detected optical signals are treated by two correlators (ALV-7004) who handle 4 detectors each and have a capacity of 7.68 billion correlations per second. The measurement and correlation data is collected and visualized by a PC software, which generates a correlation function plot, an intensity plot over time, and an error residual plot and finally a table over the averaged scattering intensities for each

detector. A post-processing for each measurement can be made to calculate the particle size distribution.

4.3 Nanoparticle Tracking Analysis (NTA)

This technique was commercialized less than ten years ago and has quickly gained popularity. Compared to Dynamic Light Scattering, it can measure at somewhat lower particle concentrations and better resolve hetero-disperse samples. It can also directly measure the particle concentration, as each individual particle in the illuminated sample volume is counted.

The equipment is simple and robust, essentially consisting of a regular optical darkfield microscope, equipped with a digital video camera, a laser and a sample cell. The liquid sample is illuminated at 90° angle to the line of view, which causes light scattering particles to appear as bright spots on a black background. The scattering intensity of an individual particle is strongly dependent on size (~R^6) in the Rayleigh scattering regime and proportional to the refractive index difference between the particle and the liquid. For particles with moderately high refractive index the detection limit is about 30-35 nm, whereas metallic particles with very high refractive index can be detected down to 10-15 nm. A video file is recorded during typically 30-60s and is subsequently processed to identify and track the particles in view. As the track has been determined, the software calculates how far the particle has moved during a certain time, then calculates the mean square displacement. From the mean square displacement in two dimensions, the diffusivity can be determined according to[115]:

$$D = \frac{\Delta z^2}{4t}$$

where Δz = mean square displacement, t = time, D = Diffusivity. From the diffusivity, the particle size can be determined with the help of the Stokes-Einstein relation.

The particle concentration of the sample needs to be low enough for individual particles to be visible in the image and tracked without interference from neighbouring particles. The upper concentration limit is about 10^{10} particles per cm^3. More concentrated samples will need to be diluted. On the lower side,

a sufficient number of particles need to be visible and tracked to get a statistically reliable result. If very few particles are visible in the field of view, a flow can be applied while the film is recorded. This allows a larger number of particles to be tracked within a certain time frame. The lower concentration limit for such measurements is about 10^6 particles per cm^3. Since the illuminated volume in the field of view is known, the number concentration of particles can be directly determined with this method. This is a very useful feature, not available in DLS and similar ensemble methods. Since every single particle is tracked and size determined, a detailed size distribution can be generated. This allows for several separate particle populations in the sample to be identified.

Since NTA can determine the size and light scattering intensity for each individual particle, it can be used to differentiate between particles of different refractive index. Experimentally it has been demonstrated that a mixture of two particle populations with the same size but with different refractive indexes can be resolved[116, 117].

A general problem with NTA is that the method is sensitive to camera and image analysis settings, which need to be carefully selected and kept the same between measurements for results to be comparable[118]. The result is also sensitive to the height in the sample at which the microscope is focused, which is a manual setting that is difficult to repeat consistently. Another source of error is that when a particle drift in and out of focus, it's imaged scattering intensity will vary. This problem is aggravated by a non-uniform intensity of the laser beam[119].

If particles with very different scattering intensities are present, it can be difficult to make a correct measurement. If settings are optimized for the strongest scatterers, the weakest ones will not be visible. If the settings are optimized for the weakest scatterers, the strongest scatterers will be visible as very large spots which are difficult to track and obscures other particles in view. This limits how heterogeneous samples that can accurately be analysed.

Commercially available hardware and software is primarily developed for size determination, and there is room for improvement concerning particle concentration and not the least refractive index determination.

4.3.2 NTA instrument - Nanosight LM10 HS (Malvern)

The instrument consists of a laser scattering microscope including a flow chamber, a syringe pump, a 488nm laser, a sCMOS camera (Hamamatsu C11440-50B) and a PC software (NTA3.2.16). The laser is located inside a laser module with a metal coated glass plate on top. A removable top plate with a second glass plate for viewing is placed on top of the illumination window. The sample is introduced into the sample chamber through a PTFE capillary (1/16" OD (ca 1.5 mm)) with the help of a syringe pump, controlled from the Nanosight software. The sample chamber is disassembled after each measurement session and cleaned with ethanol, MilliQ water and optionally SDS solution. It is also cleaned before assembly. Due to the risk of etching the optical glass, alkaline cleaning liquids should not be used. Due to the limitations of cleaning methods, there is a certain risk of cross-contamination between experiments to be aware of. There is only one sample chamber which all experimenters use.

There are several software settings to adjust for each measurement, both for the video recording and for the subsequent analysis of the video recording. To make different measurements comparable, it is recommended to change the settings as little as possible and stick to a specific protocol.

For the video recording, screen gain and Cameral Level (CL) are adjustable. Screen gain only affects the display, not the actual measurement. Camera Level is (not linearly) related to shutter time and need to be adjusted depending on the scattering intensity of the particles. If CL is too high, the camera will be saturated by the scattered light from some particles. These will be coloured blue on the screen as an indication for the operator. Large and strongly scattering particles will also be displayed and recorded as very large non-circular entities, which the software most often will not be able to track. The CL should be set low enough that only a few of the particles are blue, but high enough that all particles are visible. There are also some "advanced settings", Blur, Max Jump Distance, and Min Track length, which are automatically set by the software if not set manually.

For the analysis of the video recording, the main settings are screen gain and detection threshold. The detection threshold setting affects the results

substantially. If set too high, large particles will be overrepresented and small ones not detected.

At the advanced tab, also minimum track length can be set. This determines over how many individual frames a track must extend to be included in the output data. Default is "Auto" which means the software decides a suitable threshold (at least 5). Not setting a manual minimum track length was found to give an excess of very small particles, which are most probably artefacts. Setting the track length to at least 10 will give a smaller spread in the results. Van der Pol showed that the standard deviation would decrease substantially all the way up to a level of 30 frames as minimum track length.

4.4.1 Off-axis Digital Holographic Microscopy (DHM)

Digital Holographic Microscopy enables the creation of a 3-dimensional image of a liquid sample which also contains phase shift information. When light passes through a particle with higher refractive index than the surrounding liquid, it will slow down and acquire a phase difference compared to light not passing the particle. Vice versa, light will pass faster through a particle with a lower refractive index than the surrounding liquid – typically a gas bubble. DHM thus enables detecting gas bubbles in water and directly differentiating them from particles or droplets. The main disadvantage is however that it cannot detect as small particles as NTA and DLS.

There are several microscopy techniques to image phase differences rather than light intensity. Analog phase contrast microscopy uses a regular incoherent light source and is an old and common method to image transparent objects such as living cells, which are more difficult to see in a regular bright field image. By creating constructive interference between light scattered by the object and the background light, areas with phase shifted light will appear brighter in the image.

There are also several different methods for holographic microscopy[120], which we will not review here. Optical Digital Holographic Microscopy was first reported in the 1990s, and had a breakthrough in the 00s due to the increasing availability of better and cheaper digital cameras and laser sources, as well as computing power. The basic principle of off-axis DHM, as outlined in fig 8, is to split a laser beam into two paths, where one passes through the sample

(object beam) and one does not (reference beam). The beams are then recombined and create an interference pattern which is recorded by a digital camera. 3D- information and phase information is “hidden” in the image and is extracted by subsequent digital processing.

The second beam splitter, which recombines the two beams, is slightly rotated compared to the incoming beams. This causes the light from the two incoming beams to be directed towards the camera at a slight angle to each other. Thus, the two beams avoid hitting the camera screen at exactly the same spot, which would erase the information of interest.

The resolution is diffraction limited, just as in a regular optical microscope. This means that two particles separated by a distance which is less than about half the wavelength of the illuminating light cannot be resolved. Individual light scattering particles of smaller size than that can in principle still be detected, just like in DLS or NTA. In particular, particles can more easily be detected in the phase image than in the bright field image. The background noise does however in practice make it difficult to detect very small particles. Monodisperse Polystyrene latex particles (PSL) can be imaged down to a size of slightly less than 0.3μm, whereas more weakly scattering particles will have a somewhat higher detection limit.

4.4.2 Off-axis Digital Holographic Microscopy – experimental setup

The holographic setup is built around a regular inverted microscope (Nikon TE2000-E). The beam from a HeNe laser (633nm, Newport) is split into two paths, an object beam and a reference beam. The object beam enters an optical fiber which via a collimator illuminates the sample from above. After having passed through the sample, the object beam enters a microscope objective (Leica, 40x, NA0.75 (air) or Olympus, 40x, NA1.30 (oil)), continues through the internal optics of the microscope before it exits the microscope to be recombined with the reference beam at a beam splitter close to the front of the CCD-camera (AlliedVision, ProSilica GX1920). In addition, the beam is expanded and passed through a half-wave plate before being split by the polarizing beam splitter. The polarizing beam splitter separates the beam into two beams with orthogonal polarization. The light emitted by the laser is already linearly polarized. By adjusting the angle of the polarization before the

beam hits the beam splitter, the relative intensity of the two beams can be adjusted. A second half-wave plate in the reference beam path is used to adjust the polarization of that beam so that it is the same as that of the object beam when they subsequently meet and interfere. The experimental set-up and hologram construction has also been described in ([121]) as well as in paper 2.

The image is displayed and recorded in avi format by a custom script in LabVIEW (National Instruments). Frame rate and exposure time is selected in the script's user interface. Frame rates of up to 40 frames per second (fps) are possible, normally 20-30 fps is used. Exposure times of 5-15 ms are normally used. The exposure time is set as high as possible without oversaturating the image.

Particle/bubble dispersions are imaged in a channel with the dimensions 20x800 μm, in a microfluidic chip made of Topas (Cyclic Olefin copolymer) (Chipshop). The chip is connected via a PTFE capillary to a syringe pump which enables the sample to be viewed under flow. This makes it possible to collect images of a larger number of particles. Particle/bubble dispersions are also imaged between two clean glass slides, often with a distance of 10 μm PTFE film in between. The clean glass gives a somewhat higher image quality, but does not enable a controlled flow and does not contain the sample well.

4.4.3 Off-axis Digital Holographic Microscopy – post-processing

From the avi video file, images of both phase shift type as well as regular bright field images can be created. It is possible to digitally focus in the image and create an entire stack of images from different focus depths.

In a custom Matlab script package, "Nanosort", several operations are made. First, for each frame in the video file a correction is made for abberation in the optics and a background subtraction is made to remove spatial noise. The subtracted background is based on an average of 10 previous frames in the film. Next, a stack of phase images is created for each image frame. Thereafter, particle tracking is performed, a similar operation as in NTA (see chapter 4.3). Unlike in NTA, particles are tracked in three dimensions which is expected to give a more accurate determination of their diffusivity. For each tracked particle, its diffusivity is calculated from its mean square displacement. From the diffusivity, the particle size can be determined with the help of the Stokes-

Einstein equation. Due to uncertainty in the determination of the particle positions, the distribution of diffusivities and thus size distribution will always appear much wider than it actually is. This is the case also with the raw data from regular NTA. This is handled by a mathematical operation called convolution which makes the size distribution peaks less broad based on the knowledge that they should be less broad. When the particle tracking has been carried out, each particle has been individually identified.

For each particle, additional data can now be extracted. The integrated phase shift of each particle can be extracted from the phase images. To be clear, the integrated phase shift Φ [rad·μm^2] is the phase shift ϕ [rad] of the light passing the particle, integrated over the projected area of the particle. By extracting and averaging this value from all images along the track for the particle, a more accurate integrated phase shift can be calculated. For a spherical macroscopic particle, Φ depends on particle volume V, the difference in refractive index Δn between the particle and the dispersion medium, and the wavelength λ as follows:

$$\Phi = \frac{\Delta n V}{\lambda}$$

For particles in the Mie scattering region, this relation will however need to be adjusted with the help of Mie simulations. Note that inaccuracy in size determination will translate into inaccuracy in RI. Size and refractive index are thus not independent variables. Integrated phase shift and size are however independent variables and it is therefore useful to plot these against each other first when analysing data, this will identify different particle populations. Subsequently it can be evaluated how this translates to RI with the help of Mie simulations. As we demonstrate in paper 2, if the calculated RI based on assuming the particles to be spherical does not seem right, other assumptions can be evaluated.

4.5 Particle / bubble differentiation by pressure and vacuum treatment

4.5.1 Pressure

As discussed in chapter 3.7, pressure treatment of a solution can be used in combination with a light scattering method to differentiate between bubbles, which are destroyed by pressure treatment, from solid particles and droplets which are not.

Two different pressure vessels were used for pressure treatment of samples. The first is a plastic vessel, intended to hold water filtration cartridges. This is the same vessel which has been used for hydrodynamic cavitation experiments (see Chapter 5). It is connected to pressurized air, and equipped with a 2μm stainless steel filter (Swagelok) on the inlet. The outlet is equipped with a needle valve, enabling different rates of pressure release. Generally, liquid samples of 1.5 cm depth were exposed to 5 bar pressure for 10 minutes.

The second pressure vessel is a thick-walled stainless steel cylinder, with internal diameter 31mm and height 105mm. The inlet is connected to a tube of compressed Nitrogen, equipped with a high-pressure regulator which can provide a regulated pressure of up to 50 bar. The outlet from the steel cylinder is equipped with a needle valve (Swagelok) which is narrow enough to avoid a too violent pressure release, but does not allow for very slow decompression.

4.5.2 Vacuum

As discussed in chapter 3.8, vacuum can be used to decrease the concentration of dissolved gas in a liquid sample, which will cause bubbles to dissolve. In combination with a light scattering method it can thus be used to differentiate between particles and bubbles.

A digitally controlled vacuum pump (Büchi) was connected to a large vacuum safe glass cylinder. The sample was placed in an 8 mm glass tube and the liquid depth was about 1.5 cm. The pressure was set to 0.1 bar and kept for 24h.

5 Bubble preparation

5.0 Overview

Many methods have been devised for generating micro- and nanobubbles. They can broadly be divided into dispersion-based and oversaturation-based methods. Dispersion of gas into water can take place by injecting gas through nozzles or membranes, through high-speed stirring, through shaking, etc. Oversaturation can be achieved by saturating water at high pressure and subsequently release the pressure, by saturating water at a lower temperature and subsequently increase the temperature, through electrolysis, or through chemical decomposition of a gas releasing compound. Oversaturation can also be achieved by changing the chemical composition so that the gas solubility decreases, for example by adding inorganic salts to water or by adding water to ethanol[104]. Many methods are based on cavitation, which can be said to achieve both things. Cavitation releases gas by local subpressure and is also generating considerable dispersion.

5.1 Hydrodynamic cavitation

Hydrodynamic cavitation is carried out with the help of an equipment assembled as follows, inspired by that described in ([122]): Pressurized air is supplied from a pressure regulator via a flexible hose and passes through a stainless steel particle filter with 0.5 µm pore size and into a plastic pressure vessel. The liquid sample is placed in a glass beaker inside the vessel and the air inlet exits above the liquid surface. The outlet pipe extends almost to the bottom of the glass beaker. The outlet pipe is equipped with a needle valve which makes it possible to vary the outlet flow rate. It is possible to expose the sample to cavitation several times by pouring it back into the first beaker and pressurize the vessel again. By keeping the sample under pressure for an hour, while placed on a shaking table to ensure faster equilibration, the sample is oversaturated with air. The standard procedure is 1h at 3 bar pressure and 70 rpm shaking. This is followed by a discharge through the needle valve opened either 1.5 turns which gives a discharge rate of 0.1 l/s or 2.5 turns which gives a flow rate of 0.2 l/s. With or without oversaturation, there is always visible formation of numerous small bubbles following discharge through the needle

valve. The advantage of hydrodynamic cavitation is that it uses comparably little energy and is possible to scale up to be used for large volumes.

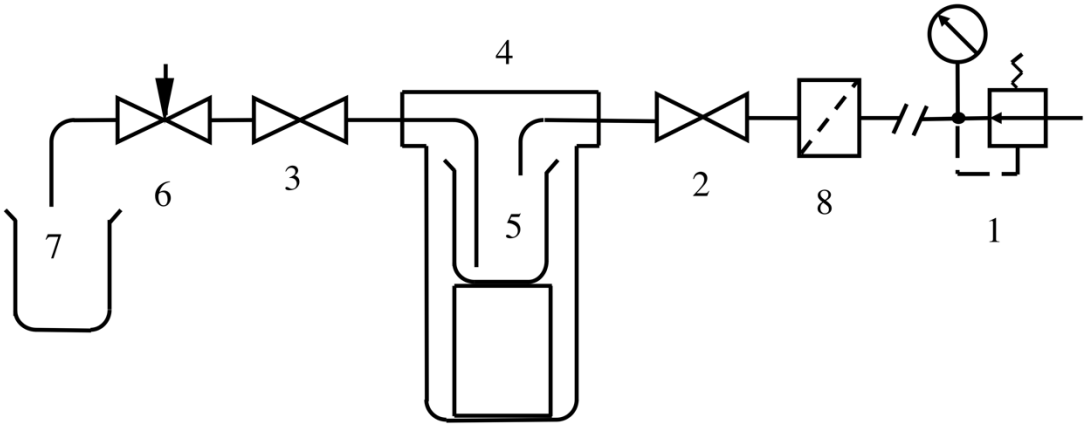

Fig 8. Equipment for hydrodynamic cavitation: (1) Pressure regulator for pressurized air; (2) and (3) Shutoff valves; (4) Pressure vessel; (5) Sample beaker; (6) Needle valve; (7) Outlet beaker; (8) Particle filter

5.2 Probe Sonication

The tip of a sonicator probe (13 mm diameter) is placed at the surface of the liquid sample, immersed only 1-3 mm. The sonicator (Sonics, Vibra-cell) has a maximum power of 500kW and a frequency of 20 kHz. Most often, 30% power (150kW) is used for 30s. As the probe is placed at the surface, it creates a vigorous stirring of the liquid which entrains and disperses a large amount of air. As the probe is used by other experimenters, the risk of cross-contamination is significant. The probe is therefore immersed in NaOH/ethanol solution for a few minutes before sonication, to ensure cleanliness. After this procedure the probe is always well wetted by pure water. Beside the potential for cross-contamination, sonication probes are known to release significant amounts of Titanium particles. This has been found to be the case also for this equipment, where a significant concentration of highly light scattering particles were detected after sonication of pure MilliQ water with a thoroughly cleaned probe. Probe sonication delivers much energy into a small volume of liquid and is thus very efficient, but it is difficult to scale up and uses much energy.

5.3 Shaking

A fast and simple method to generate bubbles in the lab is to simply shake the solution in a test tube. This may be less well defined than other methods and less powerful. It does however disperse air into the liquid very efficiently, and does generate quite strong forces in the liquid. It is not seldom used for phospholipid stabilized microbubbles.

As we found in paper 1, the stopper can be a source of contamination. Clean PTFE film is therefore used as stopper, firmly pressed against the top of the 8mm glass tube. The tube is shaken as strongly as possible up and down for 30s.

6 Summary of appended papers

6.1 Paper 1

The first paper presents a selection of the many initial experiments performed which demonstrate the great importance of contaminants in nanobubble research.

Light scattering methods such as DLS and NTA are the most commonly used to detect nanobubbles, but do not actually differentiate between bubbles and droplets or solid particles. Some papers on nanobubbles fail to address this, whereas many others use different complementary techniques to identify bubbles as actual bubbles. We report experiments where hydrodynamic cavitation of pure MilliQ water or pure salt solutions failed to generate any light scattering objects if the equipment was thoroughly cleaned, but did generate light scattering objects if that was not the case. Furthermore, experiments with bubble generation by shaking of MilliQ water or salt solutions in test tubes failed to generate any bubbles but identified several plastic stopper materials as a source of particle contamination. Air nanobubbles in water are commonly reported at concentrations of around 10^8/ml. This may sound like a high number, but for particles as small as 300nm, this corresponds to a volume fraction of only 1.3×10^{-6}. If this volume consists of solid particles with a density of 1.5 g/cm^3 instead of bubbles, it corresponds to 2mg/l. 100nm particles at the same number concentration would have a weight concentration of only 0.08 mg/l.

Experiments were also made with dissolution of very high concentrations (18-22%) of inorganic salts, which generated bubbles by lowering the air solubility in the solution. Light scattering objects were found in all solutions, but were probably mineral particles originating from the salt in most cases. Treatment of the solutions with vacuum and pressure was used to differentiate between bubbles and particles/droplets, since this is expected to destroy bubbles but leave particles unaffected. In one case this treatment did have an effect and thus one solution appeared to actually contain bubbles.

It is pointed out that in the papers which report nanobubbles in pure water or pure salt solutions, adequate contamination control is not reported in any case.

Thus, there is no experimental evidence in support of theories on nanobubble stability that is not based on adsorbed impurities. It is concluded that nanobubbles are most probably stabilized by organic contaminants at small concentrations.

6.2 Paper 2

The second paper demonstrates holographic nanoparticle tracking analysis (H-NTA) for differentiation between bubbles and particles. The bubble preparation was made in a solution of sorbitan-based surfactants (Span/Tween) in 3% NaCl, according to a known protocol. A custom-built off-axis DHM (see chapter 4.4) was used for making video recordings of the sample under flow in a 20μm high channel. Particle size (hydrodynamic diameter) was determined from the diffusivity of the imaged particles, based on tracking of their brownian motion. The phase shift of the light passing the particles was determined and different particle or bubble populations could easily be distinguished in a plot of phase shift vs hydrodynamic diameter. The method was first demonstrated for a mixture of three different polystyrene and silica particles, close in size and refractive index. The three populations, with mean sizes of 0.48, 0.40 and 0.44 μm, and with refractive indices of 1.59, 1.60 and 1.46, could readily be distinguished and their size and refractive index accurately determined. In the bubble preparation, bubbles in the range 0.3-1.5μm were easily distinguished from a present population of undissolved surfactant particles, since their phase shift is opposite that of solid particles. Following exposure to 20 bar pressure, the bubbles disappeared completely. This was also the case when the bubbles were diluted in a slightly air undersaturated NaCl solution. This was expected and in line with present understanding of surfactant stabilized bubbles. It was however surprising to find that the apparent refractive index, calculated based on assuming spherical particles, seemed to increase with size to asymptotically approach the refractive index of water. It was concluded that all but the smallest detected bubbles were actually clusters of many individual bubbles. A similar observation has previously been made on bubbles in NaCl solution[73], but it remains to be investigated how universal this phenomenon is. Detecting smaller particle/bubble sizes is unfortunately very challenging, but

nevertheless this is a method that will be very useful for further investigations on nanobubbles and in general.

6.3 Additional work

Extensive experimental work has been performed in this project which is not reported in the two papers. During the early explorative work there was no good method in place to differentiate between bubbles and particles/droplets, which made it very difficult to make stringent analysis of the many preparation methods that were explored. Impurities have been a common issue and the results on this matter reported in paper 1 is only a small selection. For instance, a high-speed stirrer used for bubble generation was found to contaminate the water with organic material and to not give a consistent stirring effect. Further, many attempts were made to generate nanobubbles in different solutions of water-soluble surfactants, mostly with negative results. It is now obvious to me that surfactants need to be water insoluble to stabilize nanobubbles, and this is supported by literature on bubbles as well as surface chemistry. However, following this line it has also been found that some poorly soluble surfactants tend to form particles rather than bubbles. Based on the theory of dynamic equilibrium and the experimental results reported in ([71]) attempts were made to form bubbles in a dilute oil emulsion, but also in this case with negative results. With the new tools now in place for detection and characterization of nanobubbles and a better understanding of the conditions necessary for their formation, I am however convinced that more rewarding investigations lie ahead in the near future.

7 Conclusions and outlook

The overarching goal of this project is to establish a method to consistently and reproducibly generate stable nanobubbles in water, without extremely high concentrations of added surfactants. For this to be possible two sub-goals are necessary to reach: understanding how nanobubbles are stabilized and establish methods of analysis to differentiate between bubbles and particles/droplets.

Concerning the stabilization mechanism, much remains to be learnt. We can conclude that some widespread ideas on nanobubble stabilization are most probably incorrect. Nanobubbles are most probably either stabilized by lipid shells or by hydrophobic particles/droplets according to the dynamic equilibrium model. This conclusion is based on extensive experimentation that shows that no stable nanobubbles are formed in very pure water or salt solutions, as well as theoretical considerations. In the field of micro- and nanobubbles as contrast agents, lipid stabilized bubbles are thoroughly studied and used commercially. However, it is a well-known fact in this field that very high concentrations of lipids (several g/l) are necessary to produce these stable bubbles. How much smaller concentrations of impurities (<10mg/l) can stabilize nanobubbles and what these impurities are remains to be determined.

Many methods have been suggested in the literature and demonstrated to selectively detect nanobubbles and differentiate them from particles and droplets[71, 77, 81, 101, 111, 123, 124]. Many of these methods have disadvantages. They may be expensive, time-consuming, and in several cases do not produce unambiguous results. We have established two practical and useful methods in this project. The first is measurement of size and concentration with light scattering methods, before and after exposure to high pressure. Bubbles are expected to be destroyed by such treatment, whereas particles or droplets remain unaffected. Pressure treatment has been reported by several authors and can be considered a relatively established method.

The second method is Digital Holographic Microscopy (DHM). This is not an established method in the nanobubble field, and it is today mostly used for imaging of living cells – not submicron particles. Despite considerable challenges, it is a method with great promise for the future, not only in the field

of live-cell imaging but also for the analysis of colloidal dispersions. It is heavily dependent on digital computation capacity and as this capacity increases year by year, DHM will become increasingly powerful. As opposed to today's work horses in nanoparticle dispersion characterization, DLS, NTA, flow cytometry, it provides information about the composition of particles, not only their size and number. If this can be achieved for particles well below 100 nm, without labeling and with short digital processing time, it is plausible that such a method eventually will replace DLS and NTA to a large extent. Reaching there remains however a tremendous challenge.

The immediate future work will focus on following up on the results in paper 2 by investigating lipid stabilized nanobubbles of different chemical compositions to see how universal the clustering phenomenon is and how much adsorbed material lipid stabilized bubbles generally have. Further work on improving the DHM/H-NTA technique will also take place in cooperation with my colleagues at Biological Physics. An attempt will be made to validate the dynamic equilibrium model for nanobubble stability, by experiments with hydrophobic nanoparticles.

List of abbreviations

DHM	Digital Holographic Microscopy
NTA	Nanoparticle Tracking Analysis
H-NTA	Holographic Nanoparticle Tracking Analysis
DLS	Dynamic Light Scattering
PTFE	Polytetrafluoroethylene (a.k.a. Teflon)

Acknowledgements

I would like to thank my supervisor Jan Swenson for letting me pursue my own project under great freedom and introducing me to the academic way after many years in industry. I would also like to thank my assistant supervisors Helén Jansson and Fredrik Höök for valuable discussions and great enthusiasm. Daniel Midtvedt, Erik Olsén and Benjamin Midtvedt for a great cooperation and the fantastic development work of the Holographic Particle Tracking technology. Thanks to Ezio Zhangelini for plenty of technical help, as well as technicians Lennart Norberg and Lasse Urholm. Thanks also to Romain Bourdes for valuable discussions, surfactant samples and lending me the probe sonicator. Thanks to all other nice, interesting, fun and helpful people at Biological Physics, our previous division Condensed Matter Physics, and elsewhere, in particular my dear colleagues in the Swenson group, Christopher, Khalid, Mansoureh and Alexander.

Finally, great thanks to my family for always supporting me, also when progress was slow.

Bibliography

1. Segers, T.; de Jong, N.; Lohse, D.; Versluis, M., Microbubbles for Medical Applications. In *Microfluidics for medical applications*, Royal Society of Chemistry: London, 2014; Vol. 36, pp 81-101.

2. Kiuri, H. J., Development of dissolved air flotation technology from the first generation to the newest (third) one (DAF in turbulent flow conditions). *Water Science and Technology* **2001,** *43* (8), 1-7.

3. Fuerstenau, M. C.; Jameson, G. J.; Yoon, R.-H., *Froth flotation: a century of innovation*. Society for Mining, Metallurgy, and Exploration: Littleton, Colorado, 2007.

4. Zhu, J.; An, H.; Alheshibri, M.; Liu, L.; Terpstra, P. M.; Liu, G.; Craig, V. S., Cleaning with Bulk Nanobubbles. *Langmuir* **2016,** *32* (43), 11203-11211.

5. Ebina, K.; Shi, K.; Hirao, M.; Hashimoto, J.; Kawato, Y.; Kaneshiro, S.; Morimoto, T.; Koizumi, K.; Yoshikawa, H., Oxygen and air nanobubble water solution promote the growth of plants, fishes, and mice. *PLoS One* **2013,** *8* (6), e65339.

6. Zhang, H.; Lyu, T.; Bi, L.; Tempero, G.; Hamilton, D. P.; Pan, G., Combating hypoxia/anoxia at sediment-water interfaces: A preliminary study of oxygen nanobubble modified clay materials. *Science of The Total Environment* **2018,** *637-638*, 550-560.

7. Liu, S.; Oshita, S.; Kawabata, S.; Makino, Y.; Yoshimoto, T., Identification of ROS Produced by Nanobubbles and Their Positive and Negative Effects on Vegetable Seed Germination. *Langmuir* **2016,** *32* (43), 11295-11302.

8. Leighton, T. G.; Coles, D. G. H.; Srokosz, M.; White, P. R.; Woolf, D. K., Asymmetric transfer of CO2 across a broken sea surface. *Sci Rep* **2018,** *8* (1), 8301.

9. Schenk, H. J.; Espino, S.; Romo, D. M.; Nima, N.; Do, A. Y.; Michaud, J. M.; Papahadjopoulos-Sternberg, B.; Yang, J.; Zuo, Y. Y.; Steppe, K.; Jansen, S., Xylem Surfactants Introduce a New Element to the Cohesion-Tension Theory. *Plant Physiol* **2017,** *173* (2), 1177-1196.

10. Georgalis, Y.; Kierzek, A. M.; Saenger, W., Cluster formation in aqueous electrolyte solutions observed by dynamic light scattering. *J. Phys. Chem. B* **2000,** *104*, 3405-3406.

11. Samal, S.; Geckeler, K. E., Unexpected solute aggregation in water on dilution. *Chemical Communications* **2001,** (21), 2224-2225.

12. Sedlak, M., Large Supra molecular structure in solutions of low molar massccompounds and mixtures of liquids - I Light scattering characterization. *J. Phys. Chem. B* **2006,** *110*, 4329-4338.

13. Fan Jin, J. L., Xiaodong Ye, Chi Wu, Effects of pH and ionic strength on the stability of nanobubbles in aqueous solutions of a-cyclodextrin. *J. Phys. Chem. B* **2007,** *111*, 11745-11749.

14. Naoyuki Ishida, T. I., Minoru Miyahara, Ko Higashitani, Nano bubbles on a hydrophobic surface in water observed by tapping-mode atomic force microscopy. *Langmuir* **2000,** *16*, 6377-6380.

15. Attard, P., Nanobubbles and the hydrophobic attraction. *Advances in Colloid and Interface Science* **2003,** *104* (1-3), 75-91.

16. Fine bubble industry association - web page. fbia.or.jp.

17. Franc, J.-P.; Michel, J.-M., *Fundamentals of cavitation*. Kluwer Academic Publishers: 2005.

18. Harvey, E. N., Physical factors in bubble formation. In *Decompression sickness*, WB Saunders Co: Philadelphia, 1951.

19. Harvey, E. N.; Barnes, D. K.; McElroy, W. D.; Whiteley, A. H.; Pease, D. C., Removal of gas nuclei from liquids and surfaces *J. Am. Chem. Soc.* **1945,** *67* (1), 156-157.

20. Fox, F. E.; Herzfeld, K. F., Gas Bubbles with Organic Skin as Cavitation Nuclei. *J. Acoust. Soc. Am.* **1954,** *26* (6), 984-989.

21. Yount, D. E.; Yeung, C. M.; Ingle, F. W., Determination of the radii of gas cavitation nuclei by filtering gelatin. *The Journal of the Acoustical Society of America* **1979,** *65* (6), 1440-1450.

22. Borkent, B. M.; Arora, M.; Ohl, C.-D., Reproducible cavitation activity in water-particle suspensions. *The Journal of the Acoustical Society of America* **2007,** *121* (3), 1406-1412.

23. Yildirim, A.; Chattaraj, R.; Blum, N. T.; Goodwin, A. P., Understanding Acoustic Cavitation Initiation by Porous Nanoparticles: Toward Nanoscale Agents for Ultrasound Imaging and Therapy. *Chem Mater* **2016,** *28* (16), 5962-5972.

24. Galloway, W. J., An Experimental Study of Acoustically Induced Cavitation in Liquids. *The Journal of the Acoustical Society of America* **1954,** *26* (5), 849-857.

25. Yount, D. E.; Strauss, R. H., Bubble formation in gelatin: A model for decompression sickness. *Journal of Applied Physics* **1976,** *47* (11), 5081-5089.

26. Brennen, C. E., *Cavitation and bubble dynamics*. Oxford University Press: New York, 1995; Vol. 44.

27. D'Arrigo, J. S., Physical properties of the nonionic surfactants surrounding gas cavitation nuclei. *The Journal of Chemical Physics* **1979,** *71* (4), 1809-1813.

28. Glaser, D. A., Some Effects of Ionizing Radiation on the Formation of Bubbles in Liquids. *Physical Review* **1952,** *87* (4), 665-665.

29. Sette, D.; Wanderlingh, F., Nucleation by Cosmic Rays in Ultrasonic Cavitation. *Physical Review* **1962,** *125* (2), 409-417.

30. Hahn, B.; Peacock, R. N., Ultrasonic cavitation induced by neutrons. *Il Nuovo Cimento (1955-1965)* **1963,** *28* (2), 334-340.

31. Iernetti, G., Cavitation Threshold Dependence on Volume. *Acta Acustica united with Acustica* **1971,** *24* (4), 191-196.

32. Liebermann, L., Air Bubbles in Water. *Journal of Applied Physics* **1957,** *28* (2), 205-211.

33. Craig, V. S. J.; Ninham, B. W.; Pashley, R. M., Direct Measurement of Hydrophobic Forces: A Study of Dissolved Gas, Approach Rate, and Neutron Irradiation. *Langmuir* **1999,** *15* (4), 1562-1569.

34. Chang, H., When water does not boil at the boiling point. *Endeavour* **2007,** *31* (1), 7-11.

35. Blatteau, J.-E.; Souraud, J.-B.; Gempp, E.; Boussuges, A., Gas Nuclei, Their Origin, and Their Role in Bubble Formation. *Aviation, Space, and Environmental Medicine* **2006,** *77* (10), 1068-1076.

36. Arieli, R.; Marmur, A., Evolution of bubbles from gas micronuclei formed on the luminal aspect of ovine large blood vessels. *Respir Physiol Neurobiol* **2013,** *188* (1), 49-55.

37. Yount, D.; Gillary, E.; Hoffman, D., A microscopic investigation of bubble formation nuclei. *The Journal of the Acoustical Society of America* **1984,** *76* (5), 1511-1521.

38. Yount, D. E., On the Elastic Properties of the Interfaces That Stabilize Gas Cavitation Nuclei. *Journal of Colloid and Interface Science* **1997,** *193* (1), 50-59.

39. D'Arrigo, J. S., Biological surfactants stabilizing natural microbubbles in aqueous media. *Advances in Colloid and Interface Science* **1983,** *19*, 253-307.

40. *Advances in Echo Imaging using Contrast Enhancement*. Springer Science: 1993.

41. Wheatley, M. A.; Cochran, M., Ultrasound contrast agents. *Journal of Drug Delivery Science and Technology* **2013,** *23* (1), 57-72.

42. de Jong, N.; Emmer, M.; van Wamel, A.; Versluis, M., Ultrasonic characterization of ultrasound contrast agents. *Med Biol Eng Comput* **2009,** *47* (8), 861-73.

43. Hernandez, C. Stabilized nanobubbles for diagnostic applications. 2018.

44. Xu, X.; Song, R.; He, M.; Peng, C.; Yu, M.; Hou, Y.; Qiu, H.; Zou, R.; Yao, S., Microfluidic production of nanoscale perfluorocarbon droplets as liquid contrast agents for ultrasound imaging. *Lab Chip* **2017,** *17* (20), 3504-3513.

45. Li, J.; Tian, Y.; Shan, D.; Gong, A.; Zeng, L.; Ren, W.; Xiang, L.; Gerhard, E.; Zhao, J.; Yang, J.; Wu, A., Neuropeptide Y Y1 receptor-mediated biodegradable photoluminescent nanobubbles as ultrasound contrast agents for targeted breast cancer imaging. *Biomaterials* **2017,** *116*, 106-117.

46. Churchman, A. H.; Mico, V.; de Pablo, J. G.; Peyman, S. A.; Freear, S.; Evans, S. D., Combined flow-focus and self-assembly routes for the formation of lipid stabilized oil-shelled microbubbles. *Microsystems & Nanoengineering* **2018,** *4*, 17087.

47. Xiao, W.; Ke, S.; Quan, N.; Zhou, L.; Wang, J.; Zhang, L.; Dong, Y.; Qin, W.; Qiu, G.; Hu, J., The Role of Nanobubbles in the Precipitation and Recovery of Organic-Phosphine-Containing Beneficiation Wastewater. *Langmuir* **2018,** *34* (21), 6217-6224.

48. Temesgen, T.; Bui, T. T.; Han, M.; Kim, T. I.; Park, H., Micro and nanobubble technologies as a new horizon for water-treatment techniques: A review. *Adv Colloid Interface Sci* **2017,** *246*, 40-51.

49. Nazari, S.; Shafaei, S. Z.; Gharabaghi, M.; Ahmadi, R.; Shahbazi, B., Effect of frother type and operational parameters on nano bubble flotation of quartz coarse particles. *Journal of Mining & Environment* **2017**.

50. Knüpfer, P.; Ditscherlein, L.; Peuker, U. A., Nanobubble enhanced agglomeration of hydrophobic powders. *Colloids and Surfaces A: Physicochemical and Engineering Aspects* **2017,** *530* (Supplement C), 117-123.

51. Calgaroto, S.; Azevedo, A.; Rubio, J., Flotation of quartz particles assisted by nanobubbles. *Int. J. Miner. Proc.* **2015,** *137*, 64-70.

52. Edzwald, J. K., Dissolved air flotation and me. *Water Res* **2010,** *44* (7), 2077-106.

53. Takahashi, M.; Chiba, K.; Li, P., Free-radical generation from collapsing microbubbles in the absence of dynamic stimulus. *J. Phys. Chem. B* **2006,** *111*, 1343-1347.

54. Yasui, K.; Tuziuti, T.; Kanematsu, W., Mysteries of bulk nanobubbles (ultrafine bubbles); stability and radical formation. *Ultrasonics Sonochemistry* **2018,** *48*, 259-266.

55. Pryor, W. A.; Houk, K. N.; Foote, C. S.; Fukuto, J. M.; Ignarro, L. J.; Squadrito, G. L.; Davies, K. J., Free radical biology and medicine: it's a gas, man! *Am J Physiol Regul Integr Comp Physiol* **2006,** *291* (3), R491-511.

56. Epstein, P. S.; Plesset, M. S., On the Stability of Gas Bubbles in Liquid-Gas Solutions. *J. Chem. Phys.* **1950,** *18* (11), 1505-1509.

57. Higgins, P., Environmental Dissolved Oxygen Values Above 100% Air Saturation. www.ysi.com, 2014.

58. Duncan, P. B.; Needham, D., Test of the Epstein-Plesset Model for Gas Microparticle Dissolution in Aqueous Media: Effect of Surface Tension and Gas Undersaturation in Solution. *Langmuir* **2004,** *20*, 2567-2578.

59. Yount, D. E., Skins of varying permeability: A stabilization mechanism for gas cavitation nuclei. *The Journal of the Acoustical Society of America* **1979,** *65* (6), 1429-1439.

60. Crane, J. M.; Hall, S. B., Rapid Compression Transforms Interfacial Monolayers of Pulmonary Surfactant. *Biophysical Journal* **2001,** *80* (4), 1863-1872.

61. Borden, M. A.; Longo, M. L., Dissolution Behavior of Lipid Monolayer-Coated, Air-Filled Microbubbles: Effect of Lipid Hydrophobic Chain Length. *Langmuir* **2002,** *18*, 9225-9233.

62. Osterroht, C., Extraction of dissolved fatty acids from sea water. *Fresenius J Anal Chem* **1993,** *345*, 773-779.

63. Hoff, L.; Foss, P. A.; Dyrstad, K.; Klaveness, J.; Rongved, P., Stabilization of Gas Bubbles Released from Water-Soluble Carbohydrates Using Amphiphilic Compounds: Preparation of Formulations and Acoustic Monitoring of Bubble Lifetime. *J Surfactants Deterg* **2011,** *14* (4), 585-593.

64. Alheshibri, M.; Craig, V. S. J., Armoured Nanobubbles; Ultrasound Contrast Agents Under Pressure. *Journal of Colloid and Interface Science* **2018**.

65. Mountford, P. A.; Sirsi, S. R.; Borden, M. A., Condensation phase diagrams for lipid-coated perfluorobutane microbubbles. *Langmuir* **2014,** *30* (21), 6209-18.

66. Kaganer, V. M.; Möhwald, H.; Dutta, P., Structure and phase transitions in Langmuir monolayers. *Reviews of Modern Physics* **1999,** *71* (3), 779-819.

67. Kwan, J. J.; Borden, M. A., Lipid monolayer collapse and microbubble stability. *Adv. Colloid Interface Sci.* **2012,** *183-184* (Supplement C), 82-99.

68. Segers, T.; Lohse, D.; Versluis, M.; Frinking, P., Universal Equations for the Coalescence Probability and Long-Term Size Stability of Phospholipid-Coated Monodisperse Microbubbles Formed by Flow Focusing. *Langmuir* **2017,** *33* (39), 10329-10339.

69. Cooke, B. D. J. a. R. C., Generation of stabilized microbubbles in seawater. *Science* **1981,** *213* (4504), 209-211.

70. Yasui, K.; Tuziuti, T.; Kanematsu, W.; Kato, K., Dynamic Equilibrium Model for a Bulk Nanobubble and a Microbubble Partly Covered with Hydrophobic Material. *Langmuir* **2016,** *32* (43), 11101-11110.

71. Sugano, K.; Miyoshi, Y.; Inazato, S., Study of Ultrafine Bubble Stabilization by Organic Material Adhesion. *Japanese Journal of Multiphase Flow* **2017,** *31* (3), 299-306.

72. Fang, Z.; Wang, L.; Wang, X.; Zhou, L.; Wang, S.; Zou, Z.; Tai, R.; Zhang, L.; Hu, J., Formation and Stability of Surface/Bulk Nanobubbles Produced by Decompression at Lower Gas Concentration. *The Journal of Physical Chemistry C* **2018**.

73. Bunkin, N. F.; Shkirin, A. V.; Suyazov, N. V.; Babenko, V. A.; Sychev, A. A.; Penkov, N. V.; Belosludtsev, K. N.; Gudkov, S. V., Formation and Dynamics of Ion-Stabilized Gas Nanobubble Phase in the Bulk of Aqueous NaCl Solutions. *J Phys Chem B* **2016,** *120* (7), 1291-303.

74. Alheshibri, M.; Qian, J.; Jehannin, M.; Craig, V. S., A History of Nanobubbles. *Langmuir* **2016,** *32* (43), 11086-11100.

75. Uchida, T.; Liu, S.; Enari, M.; Oshita, S.; Yamazaki, K.; Gohara, K., Effect of NaCl on the Lifetime of Micro- and Nanobubbles. *Nanomaterials (Basel)* **2016,** *6* (2).

76. Takahashi, M., Z potential of microbubbles in aqueous solutions - electrical properties of the gas-water interface. *J. Phys. Chem. B* **2005,** *109*, 21858-21864.

77. Ohgaki, K.; Khanh, N. Q.; Joden, Y.; Tsuji, A.; Nakagawa, T., Physicochemical approach to nanobubble solutions. *Chemical Engineering Science* **2010,** *65* (3), 1296-1300.

78. Zhang, X.; Liu, X.; Zhong, Y.; Zhou, Z.; Huang, Y.; Sun, C. Q., Nanobubble Skin Supersolidity. *Langmuir* **2016,** *32* (43), 11321-11327.

79. Kim, J. Y.; Song, M. G.; Kim, J. D., Zeta Potential of Nanobubbles Generated by Ultrasonication in Aqueous Alkyl Polyglycoside Solutions. *J Colloid Interface Sci* **2000,** *223* (2), 285-291.

80. Cho, S.-H.; Kim, J.-Y.; Chun, J.-H.; Kim, J.-D., Ultrasonic formation of nanobubbles and their zeta-potentials in aqueous electrolyte and surfactant solutions. *Colloids Surf., A* **2005,** *269* (1-3), 28-34.

81. Nirmalkar, N.; Pacek, A. W.; Barigou, M., On the Existence and Stability of Bulk Nanobubbles. *Langmuir* **2018,** *34* (37), 10964-10973.

82. Lohse, D.; Zhang, X., Surface nanobubbles and nanodroplets. *Reviews of Modern Physics* **2015,** *87* (3), 981-1035.

83. Attard, P., Pinning Down the Reasons for the Size, Shape, and Stability of Nanobubbles. *Langmuir* **2016,** *32* (43), 11138-11146.

84. Tan, B. H.; An, H.; Ohl, C. D., Surface Nanobubbles Are Stabilized by Hydrophobic Attraction. *Phys Rev Lett* **2018,** *120* (16), 164502.

85. Strasberg, M., Onset of Ultrasonic Cavitation in Tap Water. *The Journal of the Acoustical Society of America* **1959,** *31* (2), 163-176.

86. Marschall, H. B.; Mørch, K. A.; Keller, A. P.; Kjeldsen, M., Cavitation inception by almost spherical solid particles in water. *Physics of Fluids* **2003,** *15* (2), 545-553.

87. Mørch, K. A., Reflections on cavitation nuclei in water. *Physics of Fluids* **2007,** *19* (7), 072104.

88. Mørch, K. A., Cavitation Nuclei: Experiments and Theory. *Journal of Hydrodynamics, Ser. B* **2009,** *21* (2), 176-189.

89. Borkent, B. M.; Gekle, S.; Prosperetti, A.; Lohse, D., Nucleation threshold and deactivation mechanisms of nanoscopic cavitation nuclei. *Physics of Fluids* **2009,** *21* (10), 102003.

90. Israelachvili, J.; Pashley, R., The hydrophobic interaction is long range, decaying exponentially with distance. *Nature* **1982,** *300*, 341.

91. Nguyen, A. V.; Nalaskowski, J.; Miller, J. D.; Butt, H.-J., Attraction between hydrophobic surfaces studied by atomic force microscopy. *International Journal of Mineral Processing* **2003,** *72* (1-4), 215-225.

92. Meyer, E. E.; Lin, Q.; Israelachvili, J. N., Effects of Dissolved Gas on the Hydrophobic Attraction between Surfactant-Coated Surfaces. *Langmuir* **2005,** *21* (1), 256-259.

93. Ducker, W. A.; Mastropietro, D., Forces between extended hydrophobic solids: Is there a long-range hydrophobic force? *Current Opinion in Colloid & Interface Science* **2016,** *22*, 51-58.

94. Ishida, N.; Matsuo, K.; Imamura, K.; Craig, V. S. J., Hydrophobic Attraction Measured between Asymmetric Hydrophobic Surfaces. *Langmuir* **2018**.

95. Schlesinger, I.; Sivan, U., Hydrophobic Repulsion and its Origin. *arxiv.org* **2016**.

96. Schlesinger, I.; Sivan, U., New Information on the Hydrophobic Interaction Revealed by Frequency Modulation AFM. *Langmuir* **2017,** *33* (10), 2485-2496.

97. Schlesinger, I.; Sivan, U., Three-dimensional characterization of layers of condensed gas molecules forming universally on hydrophobic surfaces. *J Am Chem Soc* **2018**.

98. Pashley, R. M., Effects of degassing on the formation and stability of surfactant-free emulsions and fine teflon dispersions. *J. Phys. Chem. B* **2003,** *107*, 1714-1720.

99. Pashley, R. M.; Rzechowicz, M.; Pashley, L. R.; Francis, M. J., De-gassed water is a better cleaning agent. *J. Phys. Chem. B* **2005,** *109*, 1231-1238.

100. Aya, N.; Iki, N.; Shimura, T.; Shirai, T.; Tuziuti, T.; Yasui, K.; Kanematsu, W., Measurement of the change in the number of ultrafine bubbles through pressurization. **2014,** *9232*, 92320T.

101. Tuziuti, T.; Yasui, K.; Kanematsu, W., Influence of increase in static pressure on bulk nanobubbles. *Ultrasonics Sonochemistry* **2017,** *38*, 347-350.

102. Kovalenko, A.; Polavarapu, P.; Pourroy, G.; Waton, G.; Krafft, M. P., pH-controlled microbubble shell formation and stabilization. *Langmuir* **2014,** *30* (22), 6339-47.

103. Overton, G. D. N.; Williams, P. R.; Trevena, D. H., The influence of cavitation history and entrained gas on liquid tensile strength. *Journal of Physics D: Applied Physics* **1984,** *17* (5), 979.

104. Qiu, J.; Zou, Z.; Wang, S.; Wang, X.; Wang, L.; Dong, Y.; Zhao, H.; Zhang, L.; Hu, J., Formation and Stability of Bulk Nanobubbles Generated by Ethanol-Water Exchange. *ChemPhysChem* **2017**.

105. Tian, J.; Yang, F.; Cui, H.; Zhou, Y.; Ruan, X.; Gu, N., A Novel Approach to Making the Gas-Filled Liposome Real: Based on the Interaction of Lipid with Free Nanobubble within the Solution. *ACS Appl Mater Interfaces* **2015,** *7* (48), 26579-84.

106. Häbich, A.; Ducker, W.; Dunstan, D. E.; Zhang, X., Do stable nanobubbles exist in mixtures of organic solvents and water. *J. Phys. Chem. B* **2010,** *114*, 6962–6967.

107. Sedlak, M.; Rak, D., Large-scale inhomogeneities in solutions of low molar mass compounds and mixtures of liquids: supramolecular structures or nanobubbles? *J Phys Chem B* **2013,** *117* (8), 2495-504.

108. Zhou, C.; Cleland, D.; Snell, J.; Qi, W.; Randolph, T. W.; Carpenter, J. F., Formation of Stable Nanobubbles on Reconstituting Lyophilized Formulations Containing Trehalose. *J Pharm Sci* **2016,** *105* (7), 2249-53.

109. Tuziuti, T.; Yasui, K.; Kanematsu, W., Influence of addition of degassed water on bulk nanobubbles. *Ultrason Sonochem* **2018,** *43*, 272-274.

110. Zhang, X. H.; Li, G.; Maeda, N.; Hu, J., Removal of Induced Nanobubbles from Water/Graphite Interfaces by Partial Degassing. *Langmuir* **2006,** *22* (22), 9238-9243.

111. Hain, N.; Wesner, D.; Druzhinin, S. I.; Schonherr, H., Surface Nanobubbles Studied by Time-Resolved Fluorescence Microscopy Methods Combined with AFM: The Impact of Surface Treatment on Nanobubble Nucleation. *Langmuir* **2016,** *32* (43), 11155-11163.

112. Bohren, C. F.; Huffman, D. R., *Absorption and scattering of light by small particles*. Wiley: New York, 1998.

113. Chowdhury, D., 100 years of Einstein's theory of Brownian motion: from pollen grains to protein trains. *arXiv:cond-mat/0504610* **2005**.

114. Hassan, P. A.; Rana, S.; Verma, G., Making sense of Brownian motion: colloid characterization by dynamic light scattering. *Langmuir* **2015,** *31* (1), 3-12.

115. Saveyn, H.; De Baets, B.; Thas, O.; Hole, P.; Smith, J.; Van der Meeren, P., Accurate particle size distribution determination by nanoparticle tracking analysis based on 2-D Brownian dynamics simulation. *Journal of Colloid and Interface Science* **2010,** *352* (2), 593-600.

116. van der Pol, E.; Coumans, F. A.; Sturk, A.; Nieuwland, R.; van Leeuwen, T. G., Refractive index determination of nanoparticles in suspension using nanoparticle tracking analysis. *Nano Lett* **2014,** *14* (11), 6195-201.

117. Gardiner, C.; Shaw, M.; Hole, P.; Smith, J.; Tannetta, D.; Redman, C. W.; Sargent, I. L., Measurement of refractive index by nanoparticle tracking analysis reveals heterogeneity in extracellular vesicles. *J Extracell Vesicles* **2014,** *3*, 25361.

118. Gross, J.; Sayle, S.; Karow, A. R.; Bakowsky, U.; Garidel, P., Nanoparticle tracking analysis of particle size and concentration detection in suspensions of polymer and protein samples: Influence of experimental and data evaluation parameters. *Eur J Pharm Biopharm* **2016,** *104*, 30-41.

119. Block, S.; Fast, B. J.; Lundgren, A.; Zhdanov, V. P.; Hook, F., Two-dimensional flow nanometry of biological nanoparticles for accurate determination of their size and emission intensity. *Nat Commun* **2016,** *7*, 12956.

120. Kim, M. K., *Digital Holographic Microscopy - Principles, Techniques, and Applications*. Springer: New York, 2011.

121. Midtvedt, D.; Olsén, E.; Höök, F.; Jeffries, G. D. M., Label-free spatio-temporal monitoring of cytosolic mass, osmolarity, and volume in living cells. *Nature Communications* **2019,** *10* (1), 340.

122. Calgaroto, S.; Wilberg, K. Q.; Rubio, J., On the nanobubbles interfacial properties and future applications in flotation. *Miner. Eng.* **2014,** *60*, 33-40.

123. Uchida, T.; Oshita, S.; Ohmori, M.; Tsuno, T.; Soejima, K.; Shinozaki, S.; Take, Y.; Mitsuda, K., Transmission electron microscopic observations of

nanobubbles and their capture of impurities in wastewater. *Nanoscale Research Letters* **2011,** *6* (1), 295.

124. Alheshibri, M.; Craig, V. S. J., Differentiating between Nanoparticles and Nanobubbles by Evaluation of the Compressibility and Density of Nanoparticles. *The Journal of Physical Chemistry C* **2018**.